FRACTAL THZ SLOW LIGHT METAMATERIAL DEVICES

By

SHOICHI ITO

Bachelor of Science degree
in Electrical and Electric Engineering
Shinshu University
Nagano, Japan
2008

Submitted to the Faculty of the
Graduate College of the
Oklahoma State University
in partial fulfillment of
the requirements for
the Degree of
MASTER OF SCIENCE
December, 2010

FRACTAL THZ SLOW LIGHT METAMATERIAL

DEVICES

Thesis Approved:

Dr. Weili Zhang

Thesis Adviser

Dr. Alan Cheville

Dr. Albert T. Rosenberger

Dr. Mark E. Payton

Dean of the Graduate College

ACKNOWLEDGMENTS

I would like to express my sincere appreciation to my adviser Dr. Weili Zhang for taking me into his lab when I had anxiety about my student life. He introduced me his excellent and genial students and gave me load map to the whole new metamaterial world. He gave me lots of opportunities to learn a variety of things which cultivate my ability of thinking, judgment, observation and creativity. When I discussed my research he always listened to my speech with his keen interest and enthusiasm against research. Though I have difficulties in English conversation, he watched me with his big heart. He taught me plight as a person, not only as a researcher or engineer. I also learned importance of not afraid of challenge. I am proud to be a member in his laboratory. I really appreciate all his support.

I also thank Yongyao Chen, Wei Cao, Ran Huang, Dr. Yuping Yang, Shannon Miller, Dr. Xinchao Lu, Dr. Ranjan Singh, Dr. Jianqiang Gu and all people in the ultrafast optoelectronic laboratory for powerful suggestions and assistance. I had countless difficulties at fabrication, measurement and speculation process. They always supported me positively though they had been suspended their work. I would like to thank my family Masayasu, Naoko and Emi. They gave me unstinted assistance.

TABLE OF CONTENTS

Chapter **Page**

Chapter **Page**

LIST OF FIGURES

Figure **Page**

Figure **Page**

Figure **Page**

CHAPTER I

INTRODUCTION

1.1 Short history of metamaterial

Depending the sign, of in the relative permeability and relative permittivity, material in nature can be categorized in three groups (Fig. 1-1) [1,2]. The permittivity, permeability and index are related as [3,4]

$$n = \pm\sqrt{\varepsilon_r \mu_r} \tag{1-1}$$

where ε_r and μ_r are the relative permittivity and relative permeability, respectively [3,4]. When either permittivity or permeability is negative, the refractive index becomes imaginary and the electromagnetic wave cannot go through that material. Such materials are either metal or magnet. On the other hand, when both permittivity and permeability are positive or negative, the refractive index has a real value and the electromagnetic wave can transmit them. However, the double negative material had not been discovered until in the latter half of 20th century [4]. In 1968, V.G. Veselago predicted that "Refractive index must be negative when one has both negative relative-permittivity and negative relative-permeability" [3,4].

However, people could not find such material with negative index of refraction in nature. In 1990, J.B. Pendry *et al*. discovered that artificial materials which contain fine structures can realize whole new electromagnetic properties [2,3]. Also, in 2000, D.R. Smith *et al*. experimentally demonstrated that a substance containing certain two different types of structures can create negative index of refraction [4,6,7]. For both cases, they designed periodic structures whose dimensions are enough smaller than the wavelength of the incident electromagnetic wave. Metamaterials are thus defined that artificial structures that produce unusual electromagnetic properties not readily available in nature.

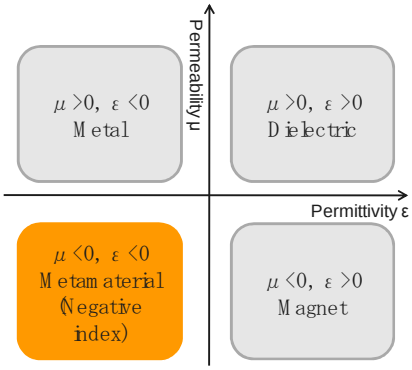

Figure 1-1 Permeability and permittivity diagram [1, 2].

In our Ultrafast Terahertz (THz) Optoelectronic Laboratory (UTOL) at Oklahoma State University, Jianqiang Gu *et al*. experimentally demonstrated the negative index of refraction in the THz frequency range in 2009. The dimensions, such as shape, length, space (gap), and periodicity etc., are important factors because they determine the electromagnetic properties [8,9]. The most famous structure is split-ring resonator (SRR) and striated wire in Fig. 1-2. The electromagnetically response of the structure can be equivalence as an electric circuit, as shown in Fig. 1-3 and their resonance frequency is decided by its dimension [1,10].

Figure 1-2 Wires and SRRs [4].

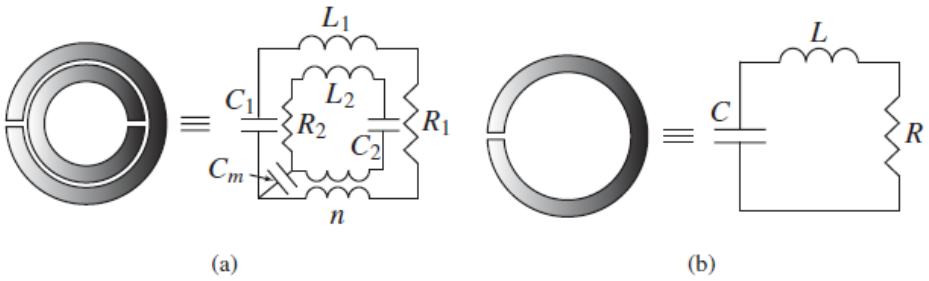

Figure 1-3 SRR and corresponding electric circuit [1]. (a) A double SRR and (b) a single SRR.

1.2 Negative refraction phenomena

Materials with negative index of refraction show unusual phenomena at Snell's law, Doppler shift, Cherenkov radiation, disagreement of group and phase velocity, and so on as described in Fig. 1-4 [4,5,11]. One of the most interesting applications is "superlens", device that performs exceeding limit of resolution [4-5]. This will benefit nanofabrication technology in semiconductor industry. People expect to have breakthrough in optical communication systems such as optical fibers, cloaking devices, and control technique in the microwave and higher frequency region.

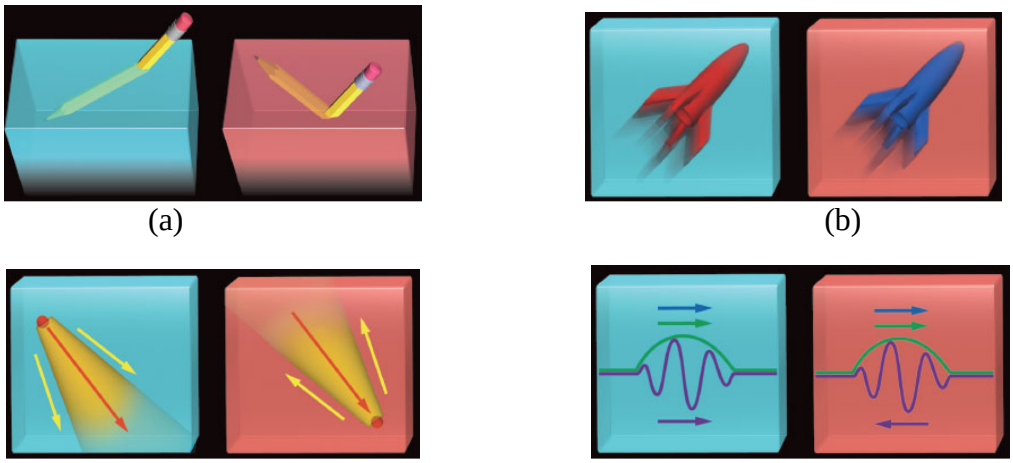

Figure 1-4 Some phenomena in material with negative refractive index [4]: (a) Snell's row, (b) Doppler effect, (c) Cherenkov radiation and (d) Group and phase velocity.
Blue background: phenomena when the material has normal refractive index, Red background: phenomena when the material has negative refractive index, (a): when the incident beam transmits from positive to negative medium, the light is bended to the same side. (b): a receding object looks bluer in material with negative index. (c): In positive index, a charge travelling faster than light creates a cone in the forward direction In negative index, the orientation of the cone is opposite. (d): In negative index, phase velocity is opposite to the group velocity and energy flow.

1.3 Phase velocity and group velocity

There are two kinds of velocities, phase velocity and group velocity [12]. Slow light is defined as situation that group velocity is slower than speed of light in vacuum, $v_g < c$ [12,13]. Phase velocity is defined as the speed of the individual waves. When a plane wave with angular frequency ω propagating through a medium with refractive index of n, it is expressed as [14]

$$\begin{aligned} \mathrm{E}(\mathrm{z},\mathrm{t}) &= \mathrm{A}\mathrm{e}^{\mathrm{i}(\mathrm{kz}-\omega\mathrm{t})} \\ &= \mathrm{A}\mathrm{e}^{\mathrm{i}\varphi}, \end{aligned} \tag{1-2}$$

where k is the wave number $\mathrm{k} = \mathrm{n}\frac{\omega}{\mathrm{c}}$ and z is the propagation direction [12]. When this wave with a constant phase point propagates a distance Δz in time Δt, we have

$$k\Delta z = \omega\Delta t. \tag{1-3}$$

The phase velocity is thus defined as [12,15]

$$\begin{aligned} v_p &= \frac{\Delta \mathrm{z}}{\Delta \mathrm{t}} \\ &= \frac{\omega}{k} = \frac{c}{n}. \end{aligned} \tag{1-4}$$

Thus, the ratio of the speed of light c to the phase velocity v_p, $n = \frac{c}{v_p}$, is called the refractive index. The phase velocity cannot carry information since they are constant.

Group velocity is defined as the speed of the wavepacket. They can carry energy and information. In the communications, we send and receive pulses which include various frequency components. Assume that there is a pulse φ composed of variety of frequencies,

$$\varphi = \frac{n\omega z}{c} - \omega t. \tag{1-5}$$

At the peak of this pulse, their Fourier components would add up in phase [12]. If there is no distortion, these components must add up in phase regardless of position z. this is expressed as

$$\frac{d\varphi}{d\omega} = 0. \tag{1-6}$$

Thus combining Eqs. (1-5) and (1-6), we have

$$\frac{dn}{d\omega}\frac{\omega z}{c} + \frac{nz}{c} - t_g = 0. \tag{1-7}$$

The group velocity v_g is defined as [12,14]

$$v_g = \frac{\mathrm{z}}{\mathrm{t_g}},$$

$$= \frac{c}{n+\omega\frac{dn}{d\omega}} = \frac{d\omega}{dk} \tag{1-8}$$

Alternatively, v_g is expressed as [12,14]

$$v_g = \frac{\mathrm{c}}{\mathrm{n_g}}, \tag{1-9}$$

$$\mathrm{n_g} = n + \omega\frac{dn}{d\omega}. \tag{1-10}$$

where $\mathrm{n_g}$ is the group refractive index. In the communication, the group velocity is extremely meaningful because the information is transmitted by light pulse and speed of group velocity acts as the speed of information. Since pulses contain various frequency components, the group velocity can be modified although phase velocities are constant.

1.4 Slow light and group delay

The speed of light in vacuum, c is approximately 2.998×10^8 m/s [16]. This constant has been one of the foremost important physical constants and has been used in Maxwell's equations. However, the recent research has showed that the velocity of light is controllable. Slow light is defined as a propagation of an optical pulse or other modulation of an optical carrier at very low group velocity [17]. Group delay is a measure of time distortion, or a measure of a slope of the transmission phase response [18]. In the Linar Time-Invariant (LTI) system theory, the input signal $x(t)$ and output signal $y(t)$ of a LTI system is expressed as

$$y(t) = h(t) * x(t), \tag{1-11}$$

where $h(t)$ is the time domain impulse response of the system [18-20]. Its frequency description is

$$Y(s) = H(s) * X(s) \tag{1-12}$$

where $H(s)$, $X(s)$ and $Y(s)$ are the Laplace transform of $h(t)$, $x(t)$ and $y(t)$, respectively [18-20]. $H(s)$ is the transfer function of the LTI system. Here, we assume that the input signal $x(t)$ is a quasi-sinusoidal signal, such as

$$x(t) = A(t)\cos(\omega t + \theta). \tag{1-13}$$

The output $y(t)$ is very well approximated as

$$y(t) = |H(j\omega)|A(t - \tau_g)\cos(\omega(t - \tau_\phi) + \theta) \tag{1-14}$$

if

$$\frac{d\log(A(t))}{dt} \ll \omega. \tag{1-15}$$

Here, τ_g and τ_ϕ are the group delay and phase delay, respectively [18]. When the input $x(t)$ is a complex sinusoid, such as

$$x(t) = e^{j\omega t}, \tag{1-16}$$

the output is expressed as [18]

$$\begin{aligned} y(t) &= H(j\omega)e^{j\omega t} \\ &= |H(j\omega)|e^{j\phi(\omega)}e^{j\omega t} \\ &= |H(j\omega)|e^{j(\omega t+\phi(\omega))}. \end{aligned} \tag{1-17}$$

Here the phase shift of the transfer function $\phi(\omega)$ is defined as [18]

$$\phi(\omega) = \arg\{H(j\omega)\}. \tag{1-18}$$

Now, the group delay τ_g and phase delay τ_ϕ are expressed as [18]

$$t_g(\omega) = -\frac{\delta\phi(\omega)}{\delta\omega}, \tag{1-19}$$

$$\tau_\phi(\omega) = -\frac{\phi(\omega)}{\omega}. \tag{1-20}$$

The group delay t_g is thus the rate of change of the total phase shift with respect to angular frequency [18,21]. The formula can also be obtained from Eq. (1-8) such as,

$$\begin{aligned} t_g &= z\frac{\delta k}{\delta\omega}, \\ &= \frac{\left(\frac{z}{\lambda_2}-\frac{z}{\lambda_1}\right)2\pi}{\delta\omega} \\ &= -\frac{\delta\phi(\omega)}{\delta\omega}. \end{aligned} \tag{1-21}$$

Slow light device which can control the group delay intentionally is promising tool to be used for high-capacity THz communication networks, all-optical information processing

and sensing devices. There are some techniques to achieve it, such as Electromagnetically Induced Transparency (EIT), photonic crystals, and so on [17]. They need to have strong dispersion in a narrow frequency region. In this work, we demonstrate the slow light or group delay by using metamaterials. In the next section, the atomic system of EIT is explained. The basic concept of EIT can be directly used to build metamaterials to mimic it and enable slow light devices.

1.5 Electromagnetically Induced Transparency to achieve slow light

1.5.1 Atomic System of EIT for slow light

Theoretically, EIT is described by using three level atomic systems [22,23]. EIT in atomic system can be explained by destructive quantum interference between the pump and the probe beams. When only the probe beam is ON, as shown in Fig. 1-5 (a), the ground and exited states are coupled and absorption occurs [22]. Here, there is no transition allowed between the ground and meta-stable state. The refractive index varies according to the absorption, as shown in Fig. 1-6. When both probe and pump beams are ON, interference between the two transitions decrease the probability of electrons existing in excited state. Since the absorptions were restrained, there is a certain frequency range among the broad absorption peak which has transparency. In this case, the refractive index has very sharp variation, as shown in Fig. 1-6. This produces long pulse delays and slow light behavior [22].

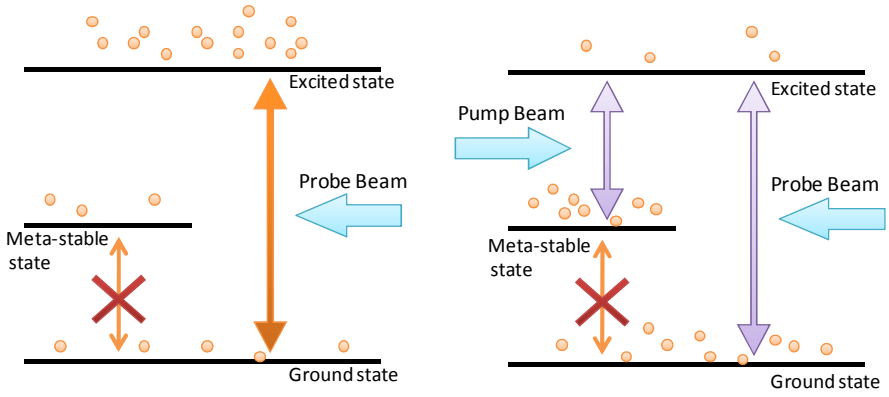

(a) (b)

Figure 1-5 Diagram of EIT [22]: (a) probe beam only and (b) probe and pump beam.

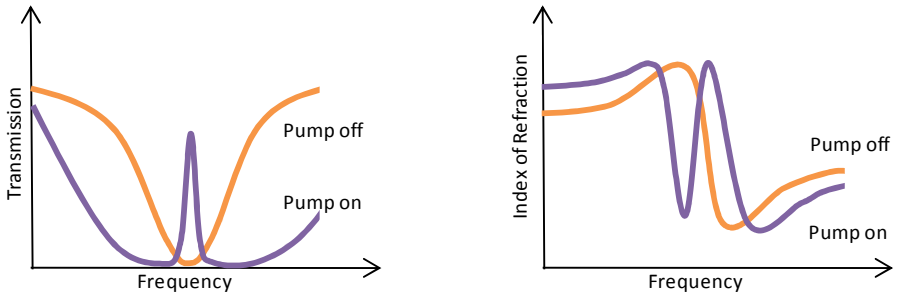

(a) (b)

Figure 1-6 Transmission and refractive index characteristics of EIT [22]: (a) Transmission and (b) Index of refraction.

1.5.2 Equivalent EIT effect

C. L. Garrido Alzar *et al*. experimentally demonstrated the EIT like phenomena by using RLC circuit [24]. This mechanical model (Fig. 1-7(a)) has two harmonic oscillators with mass m_1 and m_2, respectively. The particle 1 is connected to two springs with constant k_1 and K, respectively. The spring 1 is attached to the wall and the spring with constant K is connected to another particle 2. The spring 2 is attached to the particle 2 and wall. The

harmonic force F is applied to particle 1. The pump field is created by the coupling of these two resonators with spring K connecting them. The probe field is described as the harmonic force working on particle 1. The power which particle 1 absorbs from the probe force is measured. Fig. 1-7(b) shows the equivalent electric circuit. The right side circuit which contains a resistance R_2, capacitor C and C_2, and inductor L_2 creates pumping field. The probe field is produced by the voltage source. The left side circuit which contains resonator R_1, inductor L_1 and capacitors C_1 and C describe the atom. The resonator R_2 describes spontaneous life time decay from the excited state. The capacitor C acts as coupling between the pumping field and atom. One measures the power transferred to the circuit mesh including R_2, C, C_2 and L_2, from the voltage source V_s. When the switch is off, there is an amplitude peak whose position is determined by the value of elements. When the switch is on, the pumping resonator acts on the left circuit mesh. In the certain frequency range, the absorption caused by the circuit mesh is vanished.

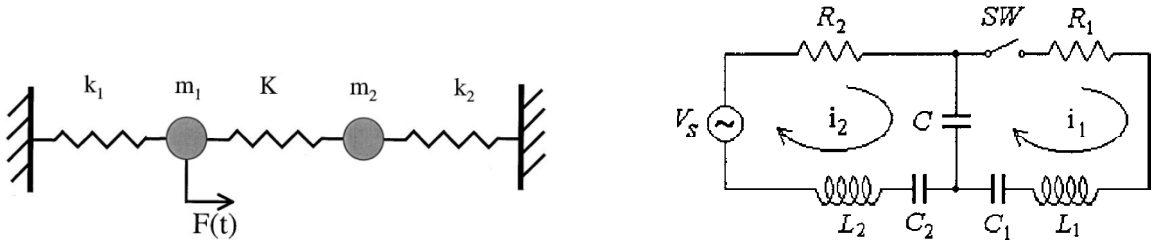

(a) (b)

Figure 1-7 EIT like phenomena in RLC circuit [24]: (a) Mechanical model and (b) Equivalent electrical circuit.

1.5.3 Slow light control using metamaterials

The combination of metamaterial and slow light is promising. In the THz regime, natural materials have difficulty to perform EIT since they have lots of energy bands and we need to set up the pump and probe beams precisely which request large-scale instruments. Natural materials thus have limitation to achieve slow light. Waveguides made up of silicon can potentially be used as the delay line system, but they costs expensively and take up space. By using the chip-scale metamaterial, we can mimic EIT [26]. We can perform slow light very simply. We can just let the incident beam passing through the slow light system and do not need instruments to focus the THz beam into the waveguide. Moreover, the time delay and the spectral region are controllable by varying the structure dimensions.

(A) Mimicking EIT on metamaterial: “Interference mode”

There are two methods to produce slow light behavior in linear optics. One is to use a technique so called breaking symmetry to lead two resonances whose resonance frequencies are close to each other [22,26]. As shown in Fig. 1-8(a), when the two arcs of the SRRs are symmetric and having the same length, the scattered wave interferes constructively and creates strong scattering. When the two arcs are asymmetric, however, the two resonators support currents oscillating in-phase, where anti-symmetric current configuration is established due to the coupling of the two resonators. The scattered wave

interferes destructively and thus scattering is eliminated or they create the reflection enhancement. This resonant mode has long lifetime due to its weak coupling to free space radiation and therefore appears to be “trapped mode” in the vicinity of the metamaterial surface. The resonant transmission peak is accompanied by steep normal dispersion. This produces low group velocities and slow light behavior. Increasing length of one arc causes further separation of the individual resonances. As another type structure, N. Papasimakis et al. investigated the fish-scale metamaterial (Fig. 1-8) [26]. The physical separation of the film creates resonance splitting. Although these resonators have dipole-like resonances, either the one on first or second layer is stronger than another. This produces opposite phase which creates anti-symmetric current configuration. Thus, the configuration interferes destructively and the scattering is eliminated at the far field.

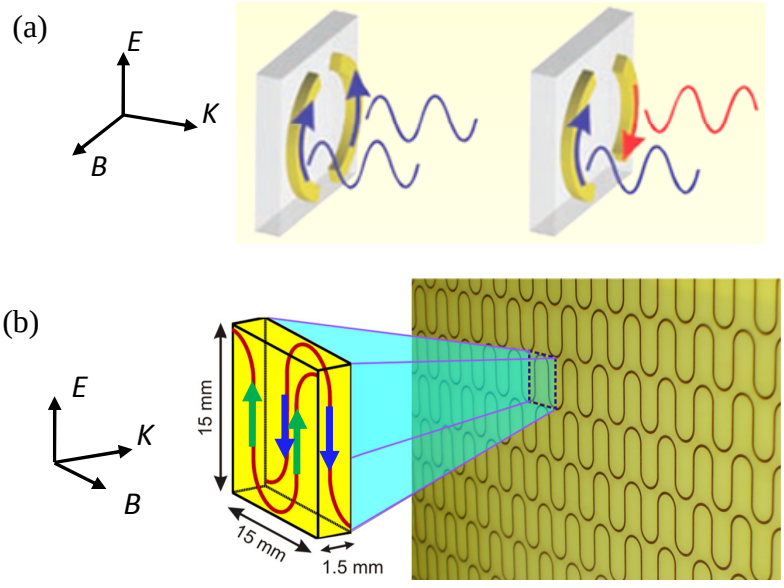

Figure 1-8 Mimicking EIT metamaterial: (a) two arcs and (b) bilayered fish-scale [22, 26].

(B) Mimicking EIT on metamaterials: the “Coupling mode”

Another method to mimic the EIT effect is to create coupling between the “bright” and “dark” eigenmode [27-29]. In 2009, Sher-Yi Chiam et. al. have experimentally demonstrated EIT using THz time domain spectroscopy (THz-TDS). They studied the mimicking EIT like phenomenon by using a planar metamaterial composed of SRRs and close rings, as shown in Fig. 1-9. For the closed outer ring, the eigenmode is called electric the dipole resonance. At the resonance frequency, a strong dipole resonance was excited on the two sides of the closed outer ring which are parallel to the electric field. Since this resonance strongly couples to the radiation field, it is called bright mode. The inner SRR does not support dipole mode around the resonance. The lowest order eigenmode of the inner SRR is the LC resonance and it couples to the free space weakly. Thus, interference of these two resonances enables a transmission window. The Q factors of the absorption dips for the sprit-ring and the closed ring are 11.3 and 1.25, respectively. The Q factors of the two resonances thus have to have a critical difference. Also, strong phase dispersion which reads large group index was measured.

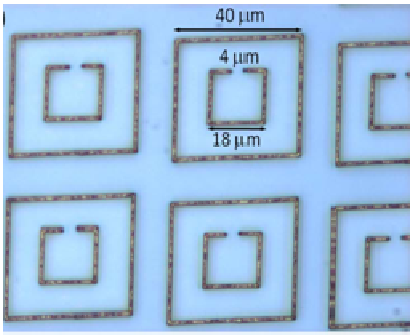

Figure 1-9 Outer closed and inner split-ring resonators to mimic EIT [27].

1.6 About This Thesis

The THz region is a new frontier. We still have difficulties to effectively generate and precisely focus the wave. Recently, researchers discovered that metamaterial can mimic EIT. They experimentally showed extreme dispersion and/or extreme group-index dispersion which of these produces slow right in the THz region. These researches extremely contribute the development of computer and communication system, semiconductor, medical and etc. Researchers have spent their focus on mechanism of the EIT−like phenomena, certain structures can show particular transmission, phase and refractive index properties, etc. In this thesis, I would like to develop this trend and focus on more about following three challenges.

(1) measurement actual time delay (Group delay)

(2) engineering of slower light by using planar metamaterials

(3) measurement of more accurate time delay

In chapter 2, fundamentals of THz- TDS and group delay are discussed.

In chapter 3, I designed a planar memtamaterial on silicon wafer. This structure is so called fractal H and referring to the interference method described in section 3.1.3 I discussed the challenges (1) and (2).

In chapter 4, I experimentally demonstrated the time delay of complementary fractal metanamterial. I discussed about the challenge (1)

In chapter 5, I show a measurement technique to achieve high spectral resolution which leads to more accurate time delay. Phase dispersion is an extremely important factor, though it occurs in a very short frequency range. I found that Mylar acts as quasi-free standing structure. It is a suitable substrate for the slow light characterization. I discussed about the challenges (1) through (3)

In chapter 6, future work based on the experimental results in chapters 3 and 5 are shown.

Finally, I strongly desire that researchers contributing this research field may overcome difficulties and breakthrough will sustain the development of our society.

CHAPTER II

TERAHERTZ TIME DOMAIN SPECTROSCOPY FOR SLOW LIGHT MEASURMEMT

2.1 THz-TDS

Figure 2-1(a) shows the optoelectronic THz beam system [30-35]. The wavelength of the femtosecond laser is 800nm. The light pulses at a repetition rate of 88 MHz are divided into two synchronized beams and reach the transmitter and receiver, respectively. The confocal quasi-optic system is bilaterally symmetric.

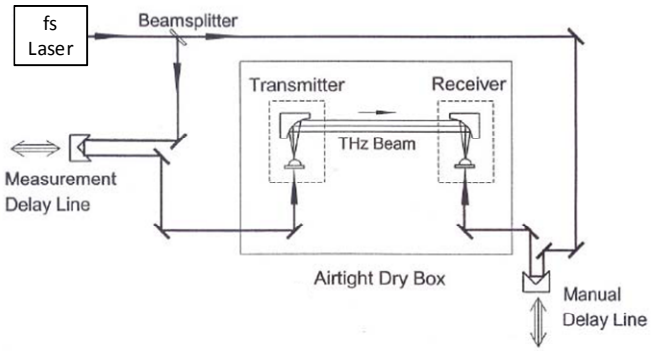

(a)

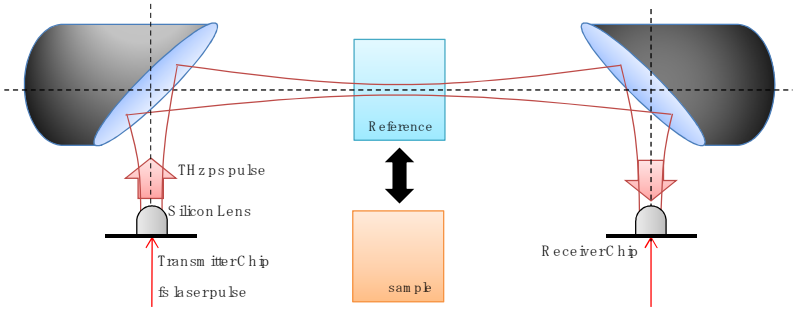

(b)

Figure 2-1 THz time-domain spectroscopy: (a) schematic diagram of the experimental setup and (b) beam system in the dry box [30-35].

The initial (excitation) light pulse with average power of 10 mW strikes the photoconductive-substrate between the two charged aluminum lines and creates carriers as shown in Fig. 2-2 [35]. These carriers are attracted by the field and this creates pulse current. At this moment, it switches into the conducting state for very short time. Such a transmission line pair is called photo conductive switch. The terahertz wave which created from this pulse current propagates along the direction perpendicular to the surface of the substrate as shown in Fig. 2-1(b). The beam of the THz pulses collimated by the 1st lens, the wave propagates and diffracts to a parabolic mirror where it is re-collimated into highly directional beam. After further propagating, the beam is incident upon the receiver, where second matched parabolic mirror focus the beam into second identical silicon. When the electromagnetic wave reaches the receiver, a electromagnetic field occurs between the transmission lines. The sampling beam strikes the photoconductive-substrate and generates carriers at an appropriate time. Then a corresponding photo current is created. The time dependence of this transit voltage is thus obtained by the measurement of this charge.

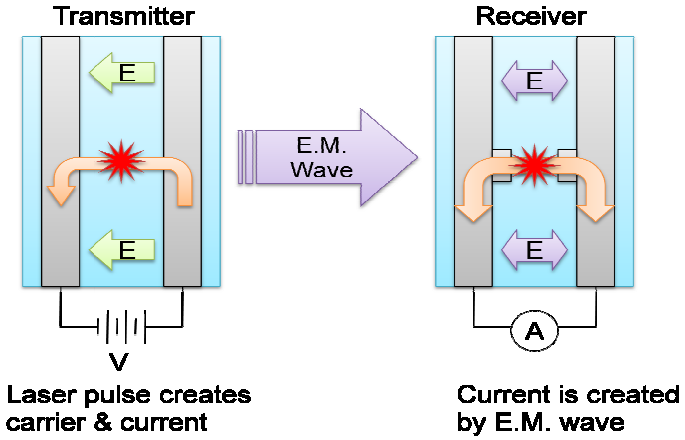

Figure 2-2 Transmitting and receiving apparatus: The orange arrows in the figure indicate the direction of current [34-35].

The relative timing between these pulses can be precisely adjusted by movement of the prism which is shown as “Measurement Delay Line” and “Manual Delay Line” in Fig. 2-3. The movable prism can be moved forward or backward at each step by a step motor. Since one step is 5μm, the total optical pass is 10μm. Thus, time which the light can travel 10μm is obtained by the following formula [34],

. (2-1)

Therefore, it can change the time that laser pulse reaches the transmitter or the THz wave reaches the receiver. Thus, the whole THz signal can be measured.

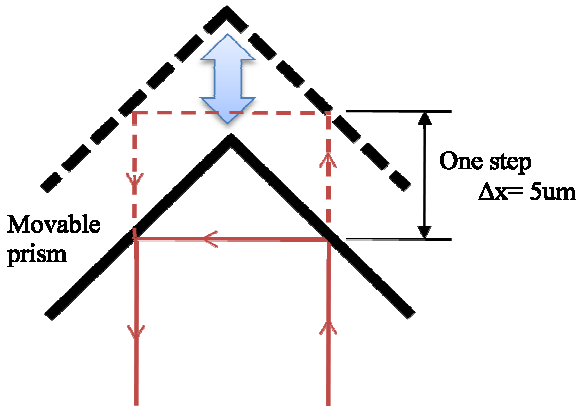

Figure 2-3 Delay-line with a movable prism [34].

In the experiment, transmission properties of sample and reference are measured each three times under room temperature.

2.2 Group Delay Measurement

Assume $E_{ref}(t)$ and $E_{signal}(t)$ are observed time profiles after passing through the reference and sample, respectively. By applying Fourier transform, the corresponding frequency domain spectra $A_{ref}(\omega)$ and $A_{smp}(\omega)$ are obtained.

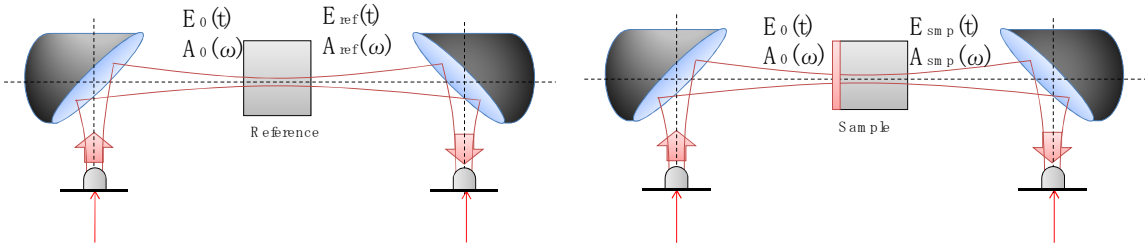

(a) (b)

Figure 2-4 Spectra acquisition: (a) reference and (b) sample data [32,34].

These frequency domain expressions $A_{ref}(\omega)$ and $A_{smp}(\omega)$ are expressed as follows [34]:

$$A_{ref}(\omega) = A_0 \exp\left(-\frac{\alpha_{ref}}{2}L\right)\exp\left[ik_{ref}(\omega)L\right], \tag{2-2}$$

$$A_{smp}(\omega) = A_0 \exp\left(-\frac{\alpha_{smp}}{2}L\right)\exp\left[ik_{smp}(\omega)L\right], \tag{2-3}$$

where α_{ref} and α_{smp} are absorption coefficients of reference and sample, respectively. $k_{ref}(\omega)$ and $k_{smp}(\omega)$ are the wave numbers of reference and sample, respectively. L is the physical thickness of the sample. Since the thickness of the metamaterial is very thin, we can assume that the total thickness is apploxximately equal to L. The wave number $k_{ref}(\omega)$ and $k_{smp}(\omega)$ can be written as follows.

$$k_{ref}(\omega) = \frac{2\pi n_{ref}}{\lambda_{ref}},\ k_{smp}(\omega) = \frac{2\pi n_{smp}}{\lambda_{smp}}, \tag{2-4}$$

where n_{ref} and n_{smp} are reflactive index of the reference and sample [34].

Ratio of these frequency domain expressions is written as [34]:

$$\frac{A_{smp}(\omega)}{A_{ref}(\omega)} = \frac{e^{-\frac{\alpha_{smp}(\omega)}{2}L}}{e^{-\frac{\alpha_{ref}(\omega)}{2}L}} \frac{e^{ik_{smp}(\omega)L}}{e^{ik_{ref}(\omega)L}}. \quad (2\text{-}5)$$

By taking absolute value of (2-5), the normalized amplitude transmission of the metamaterial can be obtained as follows.

$$T = \left|\frac{A_{smp}(\omega)}{A_{ref}(\omega)}\right| = e^{-\left\{\frac{\alpha_{smp}(\omega)}{2} - \frac{\alpha_{ref}(\omega)}{2}\right\}L}. \quad (2\text{-}6)$$

To obtain the phase shift (PT) caused by the metamaterial, we pick up the angle component [34].

$$PT = arg\left(\frac{A_{smp}(\omega)}{A_{ref}(\omega)}\right) \quad (2\text{-}7)$$

$$= (k_{smp}(\omega) - k_{ref}(\omega))L$$

$$= \left(\frac{2\pi n(\omega)}{\lambda} - \frac{2\pi}{\lambda}\right)L. \quad (2\text{-}8)$$

In this slow light measurement, phase change caused by the slow light device is measured. Assume $H_{Smp}(j\omega)$ is the transfer function of the slow light system. The phase change is expressed as [36]

$$\phi = \arg\left(H_{Smp}(\omega)\right) = \arg\left(\frac{A_{smp}(\omega)}{A_0(\omega)}\right). \quad (2\text{-}9)$$

By using the THz-TDS, we can detect $E_{ref}(t)$ and $E_{smp}(t)$, not $E_0(t)$. However, from the formula (2-2), we can obtain

$$A_0(\omega) = A_{ref}\exp\left[-ik_{ref}(\omega)L\right]. \quad (2\text{-}10)$$

By substituting (2-10) into (2-9),

$$\phi = \arg\left[\frac{A_{smp}(\omega)}{A_{ref}(\omega)}e^{ikL}\right] = \left|\frac{A_{smp}(\omega)}{A_{ref}(\omega)}\right|e^{iPT}e^{ikL}. \quad (2\text{-}11)$$

Thus ϕ can be written as

$$\phi = PT + kL. \quad (2\text{-}12)$$

The phase change caused by the slow light system ϕ is the addition of phase change caused by the slow light metamaterial and that of substrate [36].

Again, the time delay t_g can be written as [18,21]

$$t_g(\omega) = -\frac{\delta\phi(\omega)}{\delta\omega}. \tag{1-21}$$

As a simple procedure, Eq. (1-21) simply tells us that one needs to create a narrower transmission window to produce large time delay. Phase change is also a very important factor; making it larger produces large time delay. The group velocity v_g is approximately expressed as

$$v_g(\omega) \approx \frac{L}{t_g(\omega)}. \tag{2-13}$$

Thus, we can evaluate the performance of the slow light device by time delay.

There are some relationship between the time delay t_g and Q factor. The Q factor is expressed as a ratio of the resonance frequency and the full width at half-maximum (FWHM) [15, 34],

$$Q = \frac{v_0}{\delta v} = \frac{\omega_0}{\delta\omega} \tag{2-14}$$

If we assume that the nonlinear effect does not happen when the transmission window becomes very narrow, we can obtain the relationship of Q factor and time delay. By substituting (2-14) into (1-21), we have

$$t_g = -\delta\phi\,\frac{Q}{\omega_0}. \tag{2-15}$$

A important fact that Eq. (2-20) tells is obtaining high Q factor is not the method to achieve large delay. The Q factor can be large when the transmission window is placed at higher frequency. However, this does not affect the time delay at all. Again, the bandwidth is the most important factor. According to the definition of Delay-Bandwidth

Product (DBP) [37,38], the product of delay t_g and bandwidth $\delta\omega$ which is equal to phase change $\delta\phi$ is almost constant

$$t_g(\omega)\delta\omega \approx \text{constant.} \tag{2-16}$$

This tells us that obtaining narrow bandwidth is easier than large phase change.

The spectrum resolution Δf is expressed as [34]

$$\Delta f = \frac{1}{T_{total}} = \frac{1}{N\Delta t}. \tag{2-17}$$

where N is the number of sampling points (in time domain) and Δt is time resolution caused by the delay line expressed in equation (2-1). From the principle of Fourier Transform, if one wants to obtain the higher resolution Δf, the scanning time T_{total} is needed to be longer.

When an electromagnetic wave incidents upon the surface of isolated subwavelength metallic particles, resonant reflection might occur due to excitation of dipolar localized surface plasmons (DLSPs) [39,40]. The particle is polarized and dipoles are induced under the incident electric field. The field enhancement due to DLSPs leads to unique optical antennas. Assume that the length of the subwavelength rectangle structure is equal to L. When the antenna is excited with polarization of the incident electric field is parallel to the side with L, the resonance frequency f_r due to DLSPs can be approximately expressed as following,

$$f_r = \frac{c}{2L}\varepsilon_d^{-\frac{1}{2}}. \tag{2-18}$$

where c is the speed of light and ε_d is the permittivity of its substrate [40].

CHAPTER III

FRACTAL METAMATERIAL AND SLOW LIGHT MEASUREMENT

3.1 Introduction

Thus, specially designed metamaterial can mimic EIT-like phenomena and the extreme dispersion can lead to slow light [22-29]. Researchers have discussed the relationship among the structure design, transmission, phase and refractive index, etc. In this work, however, I study time delay (group delay) characterization using THz-TDS with focus on engineering slow light devices. I experimentally demonstrated that a fractal H metamaterial could enable slow light at THz frequencies. As described in section 1.5.3, there are typically two methods to mimic EIT with metamaterials and I used one of them, so called “Interference method” to obtain the transmission window. Then, I discussed the impact of dimensions on transmission and phase properties and the impact of these on the velocity of light.

F. Miyamaru *et al*. experimentally demonstrate the electromagnetic response of H-fractal structures fabricated on the silicon wafer [41]. Their fractal H structure contains fractal Hs with being scaled down connected to each ends of the original fractal H though the width is kept as constant. They investigated the transmission response, such as amplitude transmission, phase change and etc. In my work, the fractal H metamaterials with

completely different alignments and dimensions were used to demonstrate the time delay. Fractal H structures containing two different sizes are suitable to mimic EIT. This design produces a transmission window which produces time delay for both x and y directions.

3.2 Sample design and simulation

Planar fractal H structure of 200 nm thick Al metal structures are fabricated by conventional photolithography and evaporation technique on a silicon substrate (640 µm think, n-type resistivity 12 Ω cm). In Fig. 3-1, there are two fractal H structures having different dimensions. The dimensions of the larger H are a = 45 µm, b = 38 µm, w_1 = 4 µm, and w_2 = 5 µm. The dimensions of the smaller H are c = 29 µm, d = 28 µm, and w_1 = 4 µm. The periodicity P is 50µm. The orientation of the fractal Hs is such that either the THz electric field is parallel or perpendicular to x-axis, as shown in Fig. 3-1.

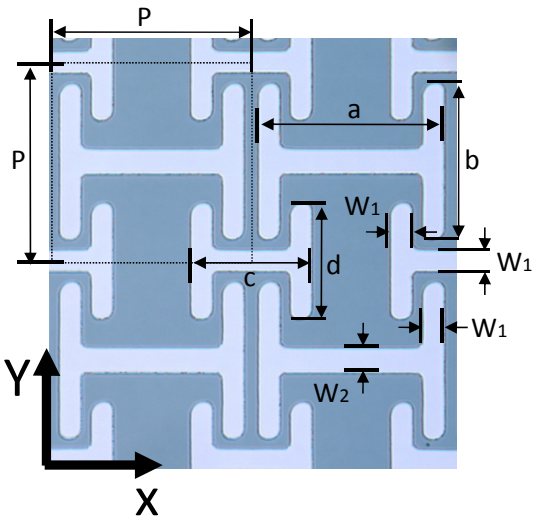

Figure 3-1 Optical image of the fractal H structure: P = 50 µm. a = 45 µm, b = 38 µm, c = 29 µm, d = 28 µm, w_1 = 4 µm, and w_2 = 5 µm.

Figures 3-2(a) and (b) shows the simulated normalized amplitude transmission for the parallel and perpendicular polarizations to x-axis, respectively. The “Larger H” or “Smaller H” means the respective oscillators. Fig. 3-3 shows the surface current (a)-(c) and electric field distribution (d)-(f) at each frequency for electric field parallel to the x-axis, respectively. Both larger and smaller H support dipole resonances and each lowest eigenmode is 0.63 and 0.99 THz, respectively. At 0.63 THz, the lower dip of the transmission window, only larger resonators are in strong resonance and are in-phase. This suggests that symmetric current on these resonators interfere constructively and create reflection enhancement. At 0.99 THz, the higher dip of the transmission window, only smaller resonators are in string resonance. They are also in-phase. This suggests that symmetric current configuration on these resonators emits electromagnetic field that interfere constructively and creates reflection enhancement. On the other hand, at 0.86 THz, the center of the transmission window, both large and small resonators are in strong resonance. The electric field distribution (Fig. 3-3 (b,e)) indicates that counter propagating currents radiates fields which interfere destructively. This eliminates scattering which has weak coupling to free space and creates a transparency window. Important fact that worth to cite is when both resonators are in resonance, each resonator is in resonant simultaneously. For electric field parallel to y-axis, similarly, the larger H and smaller H support dipole resonance with lowest eigenmodes of 1.46 and 1.77 THz, respectively (Fig. 3-4). For this polarization, when both resonators are in the strong resonance at 1.65 THz, anti-symmetric current can be seen (Fig. 3-4 (b,e)). This eliminates the scattering and creates the transparency window. In Fig. 3-2(c), extreme dispersions are created for both polarizations.

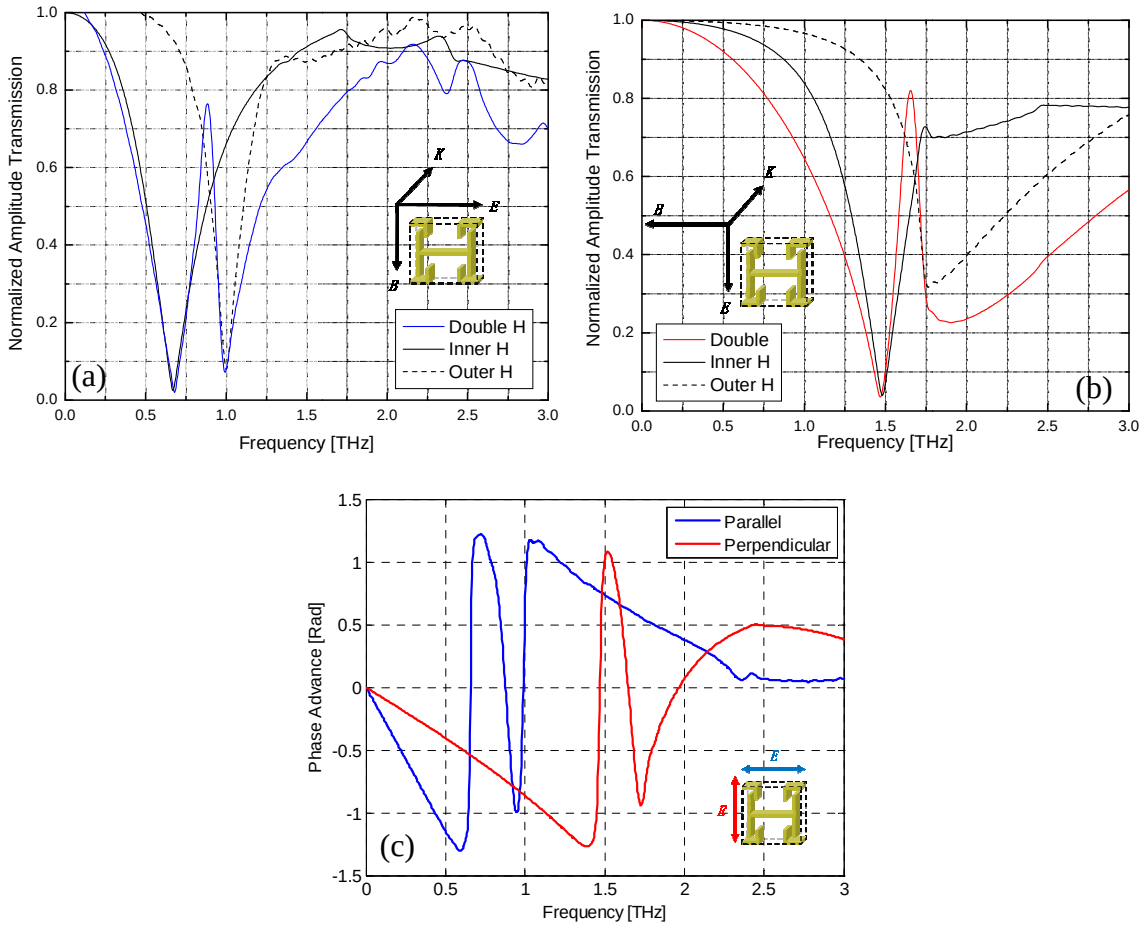

Figure 3-2 Simulation of positive fractal H on Si wafer: (a) and (b) are normalized amplitude transmissions, for parallel and perpendicular polarization, respectively. (c) is phase advance. In (a), a transmission window is found at 0.858 THz. FWHM = 0.15 THz and Q = 6.0. In (b), a transmission window is found at 1.65 THz. FWHM = 0.16 THz, Q = 10.

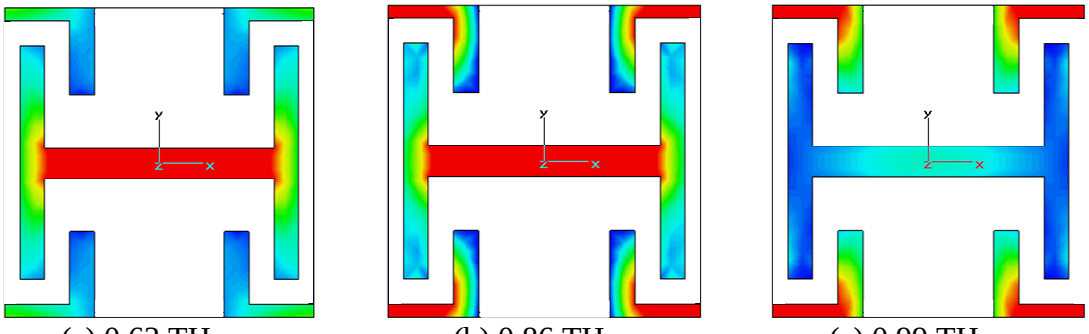

(a) 0.63 THz (b) 0.86 THz (c) 0.99 THz

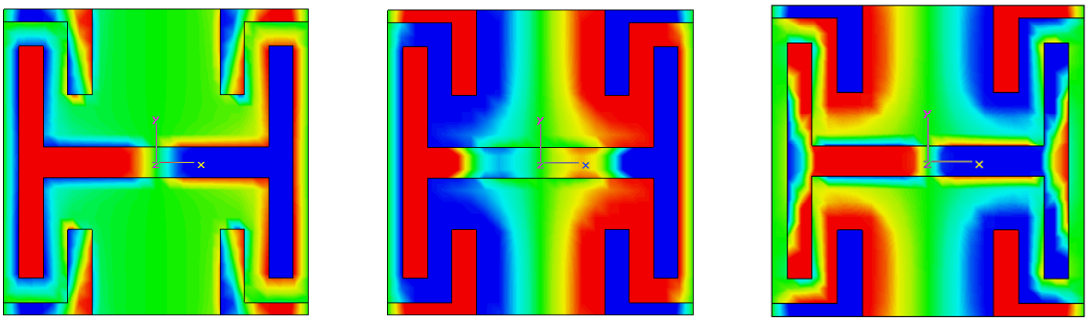

(d) 0.63 THz (e) 0.86 THz (f) 0.99 THz

Figure 3-3 Simulated surface current and electric field distribution for E // X. (a)-(c): surface current, (d)-(f): electric field; Color distribution in (a)-(c) describes current strength. They do not indicate their direction. The distribution in (d)-(f) shown by red is the positive field and blue is the negative field.

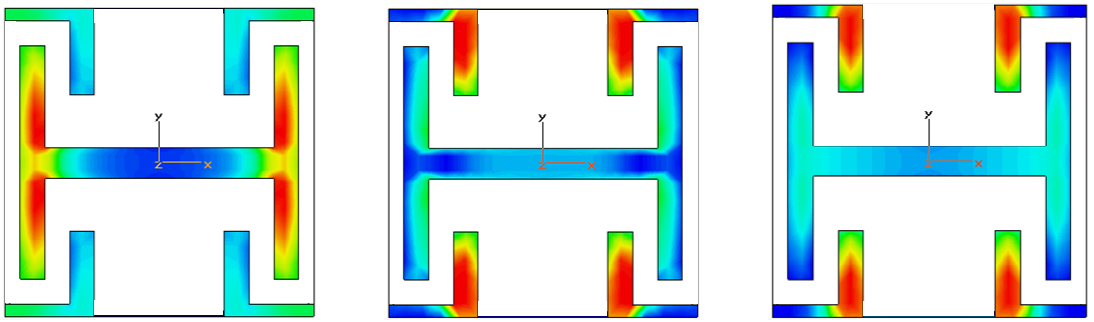

(a) 1.46 THz (b) 1.65 THz (c) 1.77 THz

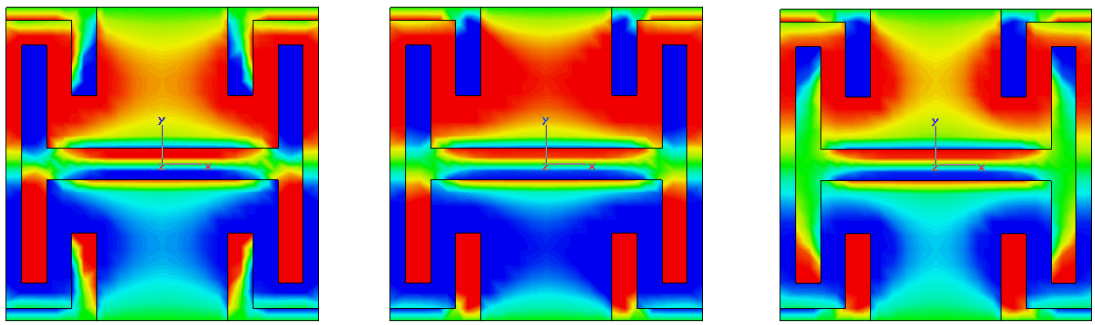

(d) 1.46 THz (e) 1.65 THz (f) 1.77 THz

Figure 3-4 Simulated surface current and electric field distribution for E // Y. (a)-(c): surface current, (d)-(f): electric field; Color distribution in (a)-(c) describes current strength. They do not indicate their direction. The distribution in (d)-(f) shown by red is the positive field and blue is the negative field.

3.3 Experimental results and discussion

The measured time domain signal transmitted through the fractal H and its frequency domain for parallel polarization are shown Figs. 3-5(a) and (b), respectively. Fig. 3-6 shows same for perpendicular polarization. Depending on dimensions of resonators which participate in the reconance, significant difference is observed in the time domain and frequency domain data.

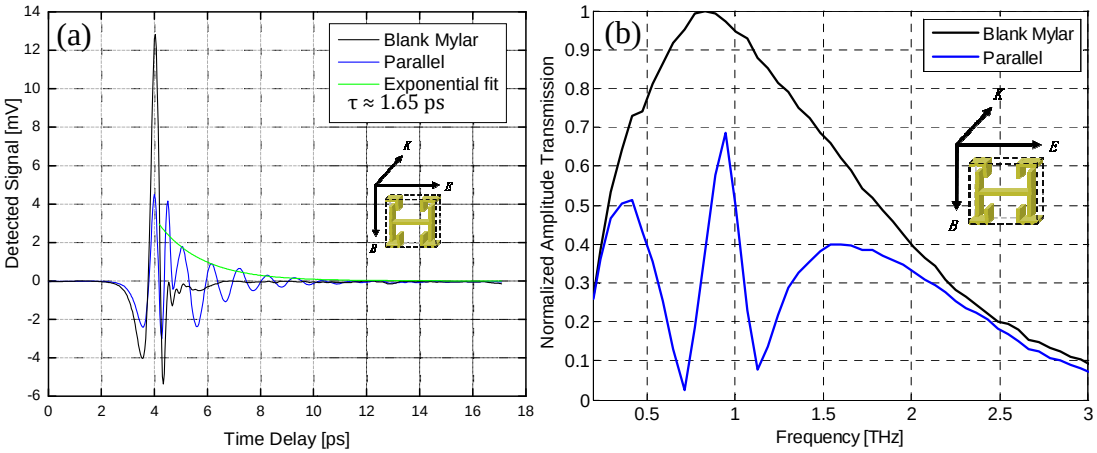

Figure 3-5 Measured signals and spectra for positive fractal H on Si substrate for E // X: (a) Signal and (b) Spectra, , .

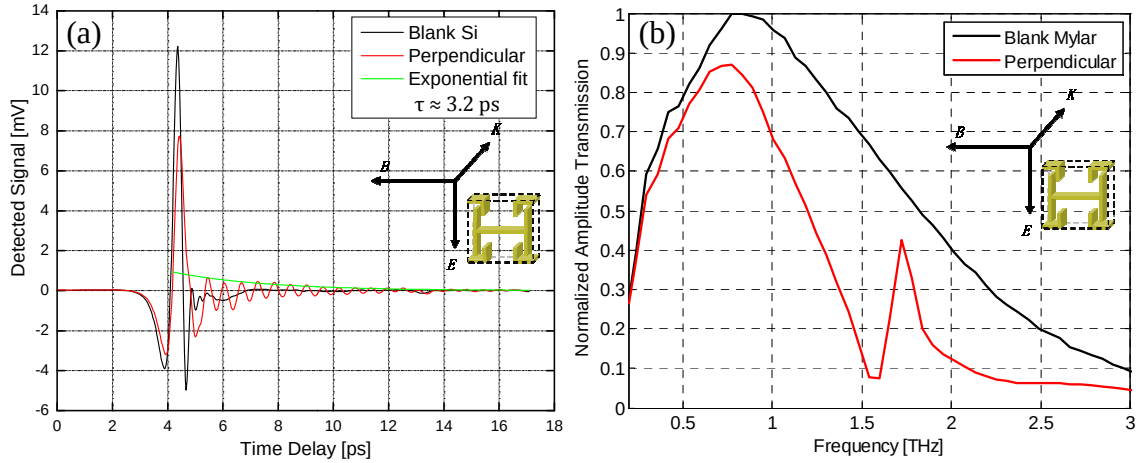

Figure 3-6 Measured signals and spectra for positive fractal H on Si substrate for E // Y: (a) Signal and (b) Spectra, , .

For observation of life time of the surface mode mediating this transmission, we used a numerical fit to the signal. The decay is treated as Lorentzian (i.e, exponential) form [42],

$$E(t) = Ae^{-t/\tau} \quad . \tag{3-1}$$

The decay time τ and time delay t_g are different factors. The decay time or life time describes how long the excited electron takes to become stable. The time delay is how long a signal delays because of material. The time domain spectroscopy shows a decaying current oscillation with a carrier frequency about 0.91 to 0.96 THz for parallel polarization. This frequency matches exactly the central frequency of the transparency window (0.95 THz) and the maximum amplitude transmission exceeds 0.7. For polarization perpendicular to the x-axis, a transparency window at 1.71 THz is observed. The maximum amplitude transmission exceeds 0.8. The time domain spectroscopy shows a slowly decaying current oscillation with a carrier frequency about 1.67 to 1.76 THz. This frequency also matches exactly the central frequency of the transparency window. These resonances are related to the interference effect of resonators with two different lengths along the polarization direction.

Their measured Q factors are 4.4 and 12.4 for electric field parallel and perpendicular to the x-axis, respectively. From the numerical fitting, the decaying time for the electric field parallel to the x-axis (1.65 ps) is smaller than that for perpendicular polarization (4.2 ps). For both polarizations, phase shifts show extreme dispersions appearing where the transparency window occurs (Fig. 3-7). For perpendicular polarization, the right side of dispersion is not as strong as that for parallel polarization. For the region of the negative phase-dispersions, it is colored blue and red for parallel and perpendicular polarization, respectively. The phase change $\delta\phi$ is 1.89 and 1.50 rad for parallel and perpendicular

polarization, respectively. The negative dispersion corresponds to the bandwidth of the transmission window almost perfectly.

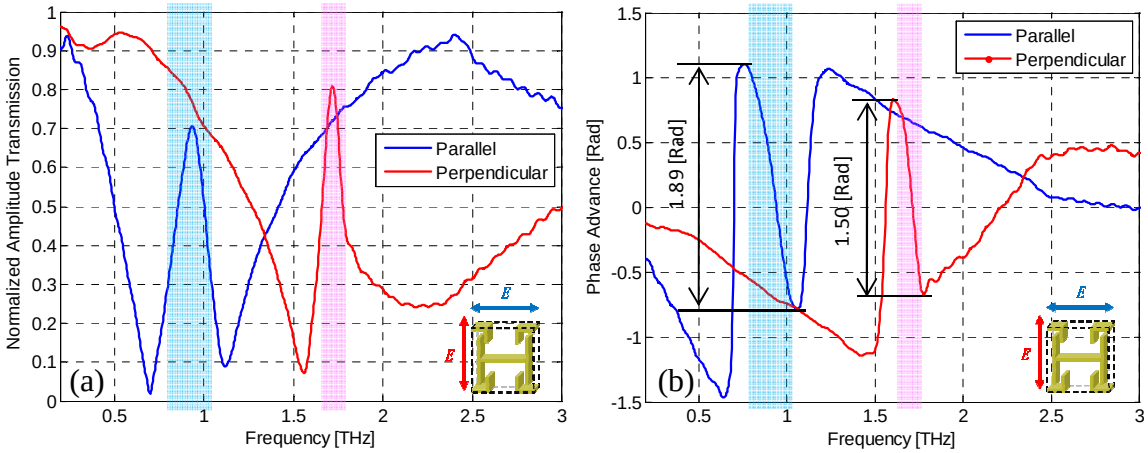

Figure 3-7 Measured normalized-spectra: (a) amplitude transmission and (b) phase advance. (zero padding applied,) For parallel polarization, a peak is observed at 0.92 THz. Its FWHM = 0.21 THz, Q = 4.4. For perpendicular polarization, peak at 1.71 THz. Its FWHM = 0.14 THz, Q = 12. Blue and red colored region correspond to negative phase dispersions.

Here, to consider the relationship between lengths of resonators and properties of the transmission window, a simulation is carried out. In this simulation, the lengths of resonators and periodicity are uniformly reduced or extended from = -5 to 35 μm although width w_1 and w_2 are kept as initial values (Fig. 3-8). From each simulation result, resonance frequency values of two dips around the transmission window are read. The results are also shown in Fig. 3-9. In the figure, circular and cross markers are corresponding to lower and higher dip positions of each transmission window, respectively. For x polarization, both higher and lower dips are seemed to obey an approximated curve. For y polarization, however, the circle and cross markers showed different components.

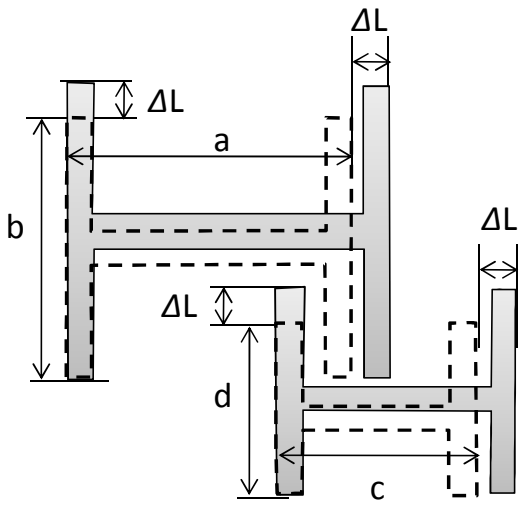

Figure 3-8 Increase the periodicity and lengths: The structures described with dashed lines are original scales. In the simulation, ΔL is extended from -5 to 35 μm with every 5 μm step.

Then, the approximate curves for the previous simulation results are considered. Again, from Eq. (2-18), the resonance frequency of rectangle metamaterials due to the DLSPs is expressed as [39,40]

$$f_r = \frac{c}{2L}\varepsilon_d^{-\frac{1}{2}}. \tag{2-18}$$

For the fractal H structure, we made an assumption that this fractal H structure which is the combination of the rectangular resonators potentially shows similar resonant properties to that of the above rectangle structure. More concretely, it can be assumed that there are two rectangular resonators for x orientation and four rectangular resonators for y direction (Fig. 3-10). Then, each resonator individually satisfies the above principle. In fact, the fractal H metamaterial has two resonance frequencies and a transmission window placed between them. These resonance frequencies of lower and higher dips have been obtained by previous simulations. As a result, these resonance frequencies for silicon substrate $f_{rx_{Si}}$ and $f_{ry_{Si}}$ are approximately explained as

—— ¯ , for E // X (3-2)

— ¯ , for E // Y (3-3)

where a and b are constants and is the dielectric constant of Si (=11.4 at 0.1THz).

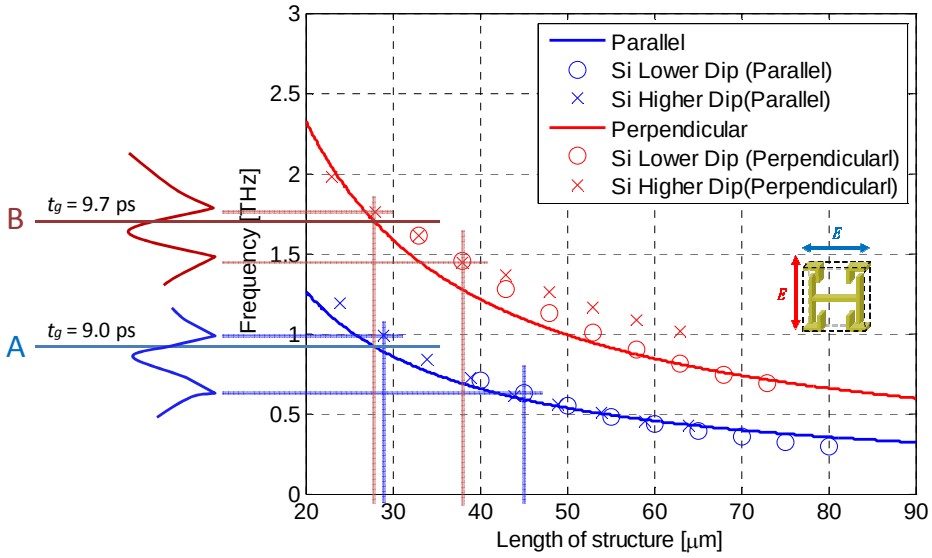

Figure 3-9 Resonance frequency approximation of fractal H on silicon: solid lines are obtained from equations (3-3) and (3-4). The circle and cross markers are obtained by simulations. "Lower Dip" and "Higher Dip" suggest left and right edges of the transmission window, respectively. For y polarization, markers of "Lower Dip" and "Higher Dip" have different approximate curves. A and B with solid lines are measured center frequencies of parallel and perpendicular polarization, respectively.

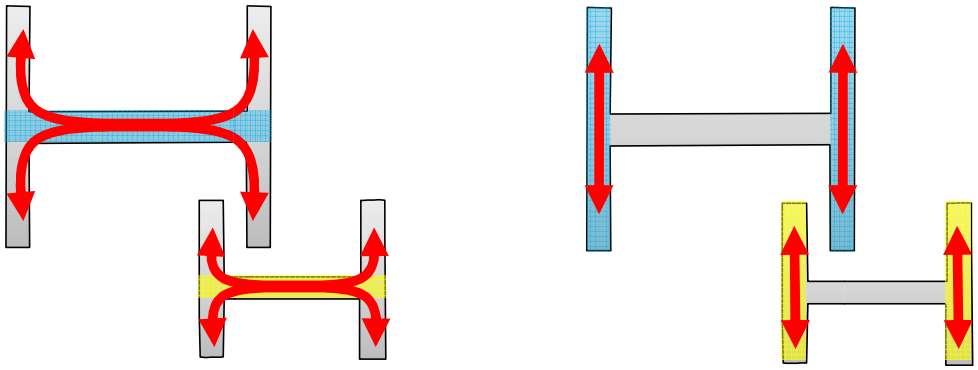

(a) (b)

Figure 3-10 Rectangular resonators in fractal H structure: (a) parallel and (b) perpendicular polarization. The red arrows suggest the current flows. For parallel polarization, the lengthwise resonators are needed to be taken in to account.

For parallel polarization, the two longitudinally-arranged rectangles strongly contribute to the dipole resonance (Fig. 3-8 (a)). Therefore, the effective length contributing to this resonance is needed to be taken into account. For larger H structure, the effective length is approximately equal to a+b μm or 1.84a. For smaller H structure, the effective lengths are approximately equal to c+d μm or 1.97c. Thus, we put 1.9L, the average of these effective lengths, for the denominator of (3-2). On the other hand, for perpendicular polarization, we can consider that the contribution of the laterally-arranged resonator to the longitudinal rectangles is sufficiently-small (Fig. 3-8 (b)). Thus, we have L for the denominator of (3-3). The curves calculated by these equations are show in Fig. 3-9 when the constants a ≈ +0.05 THz, the constant b ≈ 0.1 THz. Strictly speaking, there are mainly two factors that increase the accuracy of these fitting curves. One is that the average effect of the substrate and free-space is needed to be taken into account. Another is that we need two approximation curves to describe the resonance frequencies of the two resonators individually for the perpendicular polarization since the contribution of the laterally-arranged resonator placed in each H structure cannot be ignored.

As consequence, the importance of this figure is that if one wants to have narrow bandwidth peak, making the lengths of two resonators large (keep the ΔL constant) might give that output. However, it is worth to recite that achieving narrower bandwidth sometime does not directly produce large time delay. Although extending the length of resonator creates narrow bandwidth, its phase advance might not be so critical. In fact, varying lengths did not produce strong phase dispersion in this simulation.

Figures 3-11(a) and (b) show the measured time delay for electric field parallel and perpendicular to the x-axis, respectively, that obtained by using Eq. (1-21). The theoretical value of time that beam passes through the Si substrate is approximately 7.26 picoseconds. Around the 0.95 THz in (a), where the transmission window occurs, maximum 1 ps slow light (velocity = 2.64×10^8 [m/s]) is observed. In (b), slow light (velocity = 2.24×10^8 m/s) is also observed at 1.71 THz. According to Eq. (2-16) which is

$$t_g(\omega)\delta\omega \approx \text{constant}, \tag{2-16}$$

i.e. the product of delay t_g and bandwidth $\delta\omega$ is almost constant [37,38].

From this experiment, the bandwidth for parallel polarization is broader than that of the perpendicular one. This causes time delay of the latter slower than that of the former.

$$\delta\omega_A > \delta\omega_B \quad \Leftrightarrow \quad t_{g_A} < t_{g_B}. \tag{3-4}$$

Slowness of these is strongly related to the negative phase dispersion in the whole extreme dispersion. Moreover, these curves contain noise like oscillations whose amplitude is relatively high. It makes these outputs not trustable. On the other hand, at the dips placed at 0.70 and 1.11 THz in (a) and at 1.56 THz in (b), negative time delays are observed. Their time delay was faster than that in the blank silicon water and expressed as [12],

$$t_g > c. \tag{3-5}$$

Thus, the negative phase dispersion creates slow light. Instead, the positive phase dispersion enables the fast light.

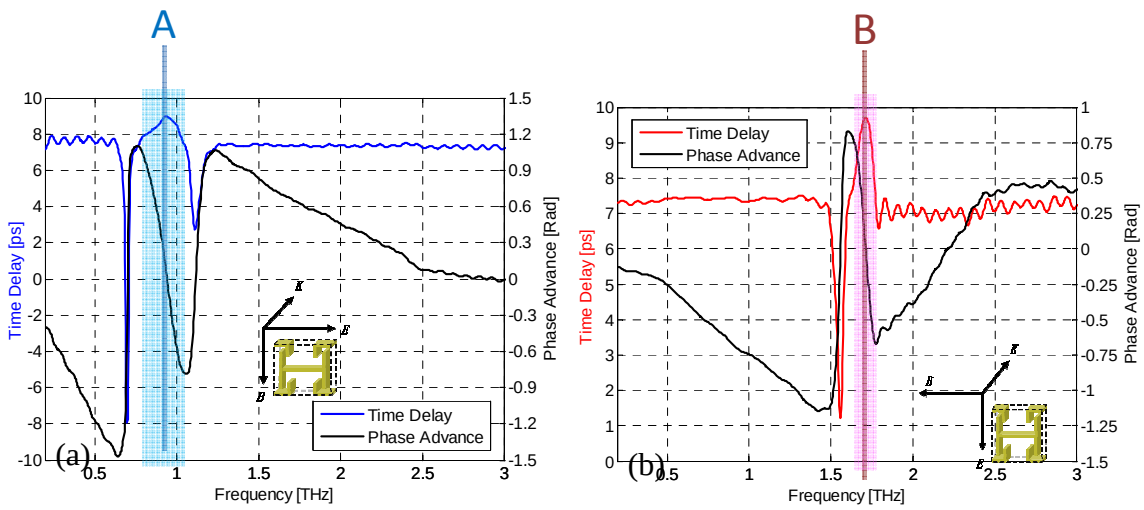

Figure 3-11 Measured time delay and phase advance: (a) parallel and (b) perpendicular polarization. For parallel polarization, dip at 0.70 THz: time delay = -7.9 ps, hill at 0.94 THz: time delay = 9.0 ps (Solid line A), dip at 1.11 THz: time delay 2.74 ps. For perpendicular polarization, dip at 1.56 THz: 1.22 ps, peak at 1.71 THz; time delay = 9.70 ps (Solid line B). Blue and red colored region correspond to negative phase dispersions.

3.4 Summary

We experimentally demonstrated slow light of fractal H metamaterial. This slow light device produces a transmission-window for each polarization. Narrow bandwidth and strong phase dispersion are key factors to produce large time delay. Especially, ONLY negative dispersion within the extreme dispersion contributes to slowness. Edges (or dips) and amplitude of transmission window does not directly affect the slowness. However, the device showed low Q factor and the detected slow light was not remarkable. We could conquer this problem by expanding lengths of resonators since this creates narrow bandwidth. Seeking high Q factor is one method to obtain the narrow bandwidth. However, we need to have narrow bandwidth and strong phase dispersion as well.

CHAPTER IV

COMPLEMENTARY FRACTAL METAMATERIAL AND TIME DELAY

4.1 Introduction

Positive type structures have been used for most of previous work to mimic EIT since interference or coupling between the resonators is the key technique. In this chapter, I experimentally demonstrate a complementary fractal H structure which has the same dimensions as used in the previous chapter. For the compliantly structure, frequencies of the transmission dip with the incident polarizations rotated 90 degrees are seen at the same frequencies as those of transmission peaks in the positive fractal structure. This is called the Babinet's principle [42-44]. Extreme negative-dispersion contributing slow light is not found.

4.2 Sample Design and Simulation

Complementary fractal Hs of 200 nm thick Al metal structures are fabricated by conventional photolithography and evaporation technique on a silicon substrate (640 μm

think, n-type resistivity 12 Ω cm). Fig. 4-1 shows the complementary structure. Dimensions are exactly equal to these of the positive type structure. The dimensions of the larger H are a = 45 μm, b = 48 μm, w_1 = 4 μm, and w_2 = 5 μm. The dimensions of the smaller H are c = 29 μm, d = 28 μm, and w_1 = 4 μm. Periodicity P is 50μm.

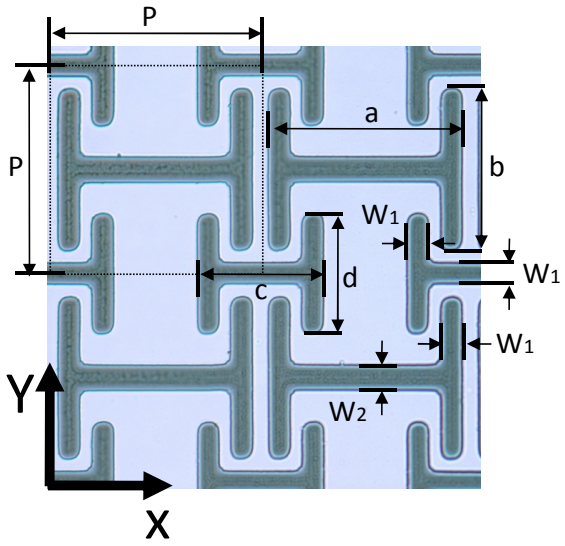

Figure 4-1 Optical image of the complementary fractal H structure: P = 50 μm. a = 45, b = 48, c = 29, d = 28, w_1 = 4 and w_2 = 5 μm.

Figure 4-2 shows the simulated spectra of the negative fractal H on Si substrate. Both spectra agree with the measured spectra, although blue shift is observed. Also, Figs. 4-3 and 4-4 show the distribution of simulated surface current and electric field for polarizations parallel and perpendicular to the x-axis, respectively. When a resonator, outer and/or inner fractal H, in the positive fractal structure is in resonant, the electric field between the gaps, i.e. the space between neighboring resonators, is enhanced. At this time, the corresponding area of the complementary structure has high surface current distribution. Similarly, when electric field distribution in the complementary structure is largely located around a resonator, the corresponding resonator in the positive structure

has high surface current distribution. These observations agree with the resent work by Carsten Rockstuhl et al [43] and of Hou-Tong Chen *et al* [44]. Thus, for the positive structure, the incident wave induces surface current on resonator and charges are accumulated at the edge. The gap produces enhanced electric field. On the other hand, for the complementary structure, the incident wave induces current on surrounding metal and charges are sprinkled in various areas. Therefore, this phenomenon is caused by electric response, not magnetic or magneto-electronic response.

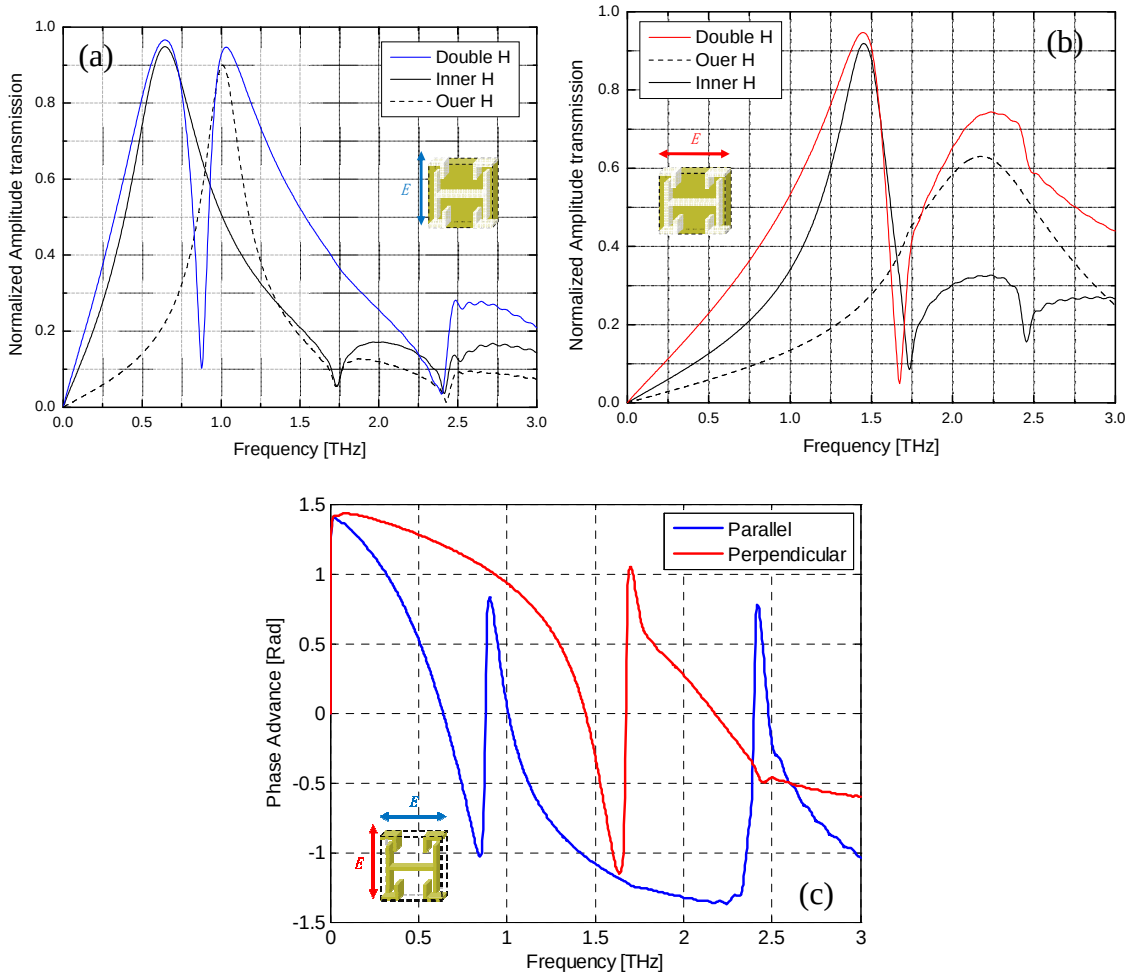

Figure 4-2 Simulated spectra of negative fractal H on Si substrate: (a) Parallel, (b) Perpendicular, and (c) Phase advance. For parallel polarization, peak at 0.88 THz: FWHM = 0.14 THz and Q = 10.5. For perpendicular polarization, peak at 1.67 THz: FWHM = 0.17 THz and Q = 12.

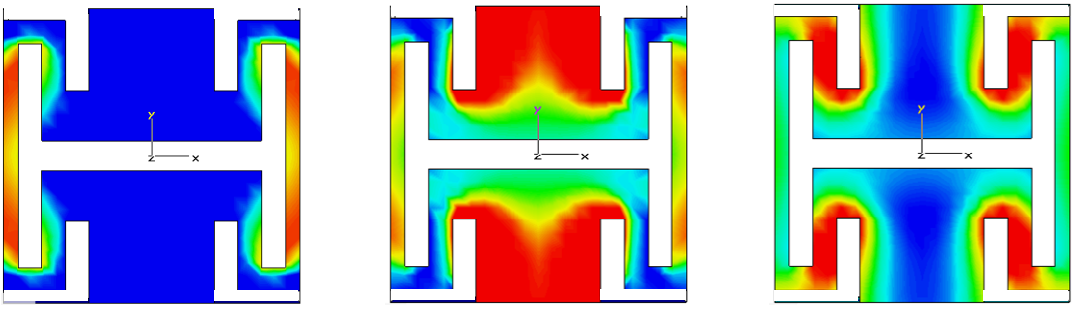

(a) 0.65 THz (b) 0.79 THz (c) 1.03 THz

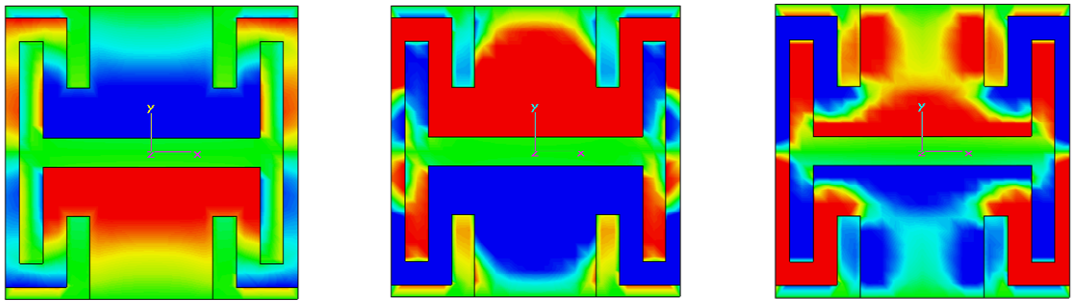

(a) 0.65 THz (b) 0.79 THz (c) 1.03 THz

Figure 4-3 Simulated surface current and electric field distribution of complementary fractal H metamaterial for E // X: (a)-(c): surface current, (d)-(f): electric field; Color distribution in (a)-(c) describes current strength. They do not indicate their direction. The distribution in (d)-(f) shown by red is the positive field and blue is the negative field.

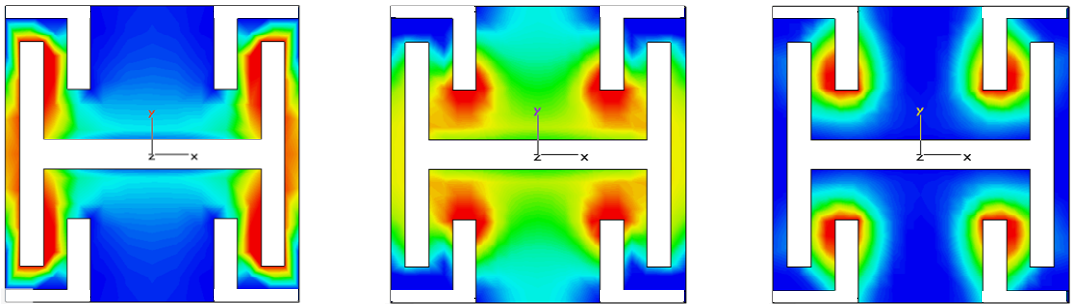

(a) 1.45 THz (b) 1.67 THz (c) 2.45 THz

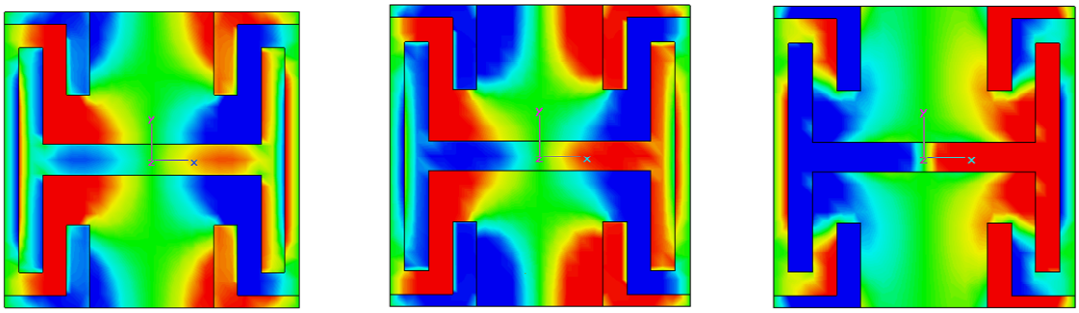

(d) 1.45 THz (e) 1.67 THz (f) 2.45 THz

Figure 4-4 Simulated surface current and electric field distribution of complementary fractal H metamaterial for E // Y: (a)-(c): surface current, (d)-(f): electric field; Color distribution in (a)-(c) describes current strength. They do not indicate their direction. The distribution in (d)-(f) shown by red is the positive field and blue is the negative field.

4.3 Experimental Result and Discussion

The transmission spectra of the negative (complimentary) type of fractal H structures are also experimentally investigated. Figs. 4-5 and 4-6 show the measured electric pulse and corresponding FFT spectra for the electric field parallel and perpendicular to the x-axis, respectively. Fig. 4-5(b) shows a dip, or so called absorption window, centered at 0.92 THz for polarization parallel to the x-axis. The Q factor for this dip is 7. In Fig. 4-6(b), an absorption window located at 1.7 THz. Also, the Q factor for the polarization perpendicular to the x-axis is 14. These time domain spectra show the decay time of 1.40 and 1.74 ps for the parallel and perpendicular polarization, respectively. These time domain data for x polarization show the decaying current oscillation with carrier frequency from 0.86 to 0.97 THz. The frequencies match to these of each absorption window (dip). For the perpendicular polarization, the decaying current oscillation with carrier frequency is about 1.6 THz and this also matches to the frequency of the absorption window. Fig. 4-7 shows normalized amplitude transmission and phase advance. Zero padding has been applied for these figures. For the complementary structure, the ratio of metal area against one unit cell is 0.68 (0.42 for the positive). However, the energy of the incident wave is not refracted from the surface or confined in the subwavelength slit very much [43]. The dip position observed in each spectrum corresponds to peak position in the positive type structure. For both polarizations, a strong normal dispersion appears within the corresponding absorption window.

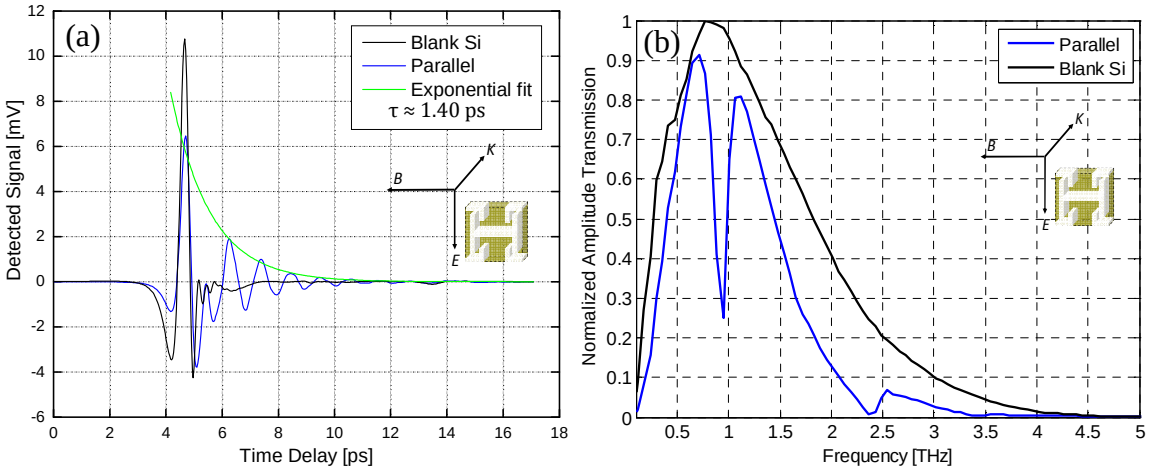

Figure 4-5 Measured signals for complementary structure on single Si substrate for parallel polarization: (a) Measured electrical pulse and (b) Measured spectra.

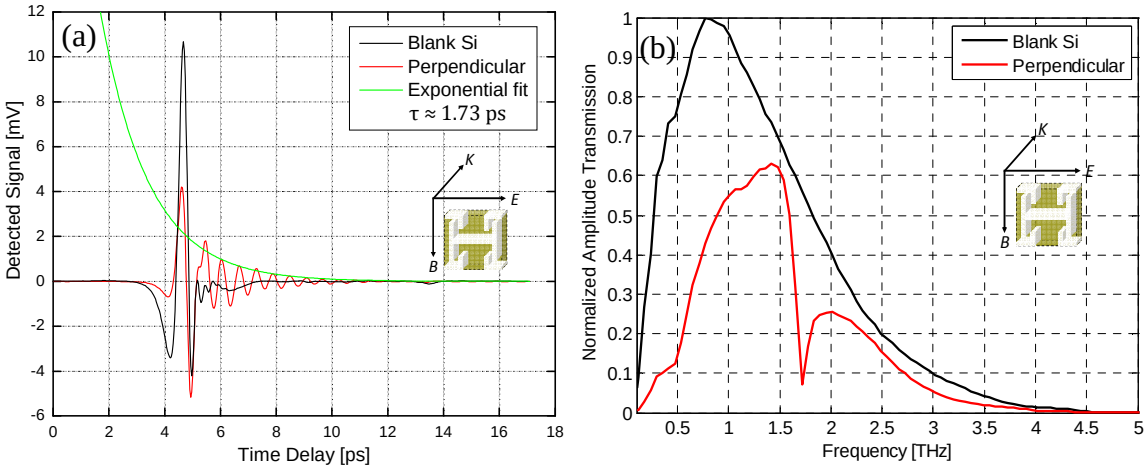

Figure 4-6 Measured signals for complementary structure on single Si substrate for perpendicular polarization: (a) Measured electrical pulse and (b) Measured spectra.

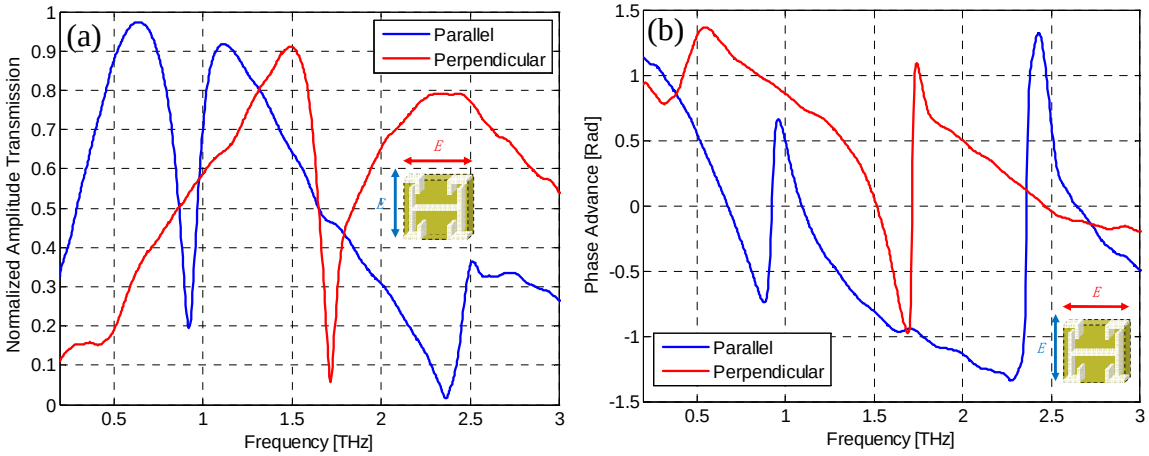

Figure 4-7 Measured normalized amplitude and phase of complementary fractal H on Si wafer: (a) Normalized amplitude transmission and (b) Phase advance. For parallel polarization, peak at 0.92 THz: FWHM = 0.14 THz and Q = 7.0. For perpendicular polarization, peak at 1.72 THz: FWHM = 0.16 THz and Q = 14.

Figures 4-8 shows measured time delay and phase advance for parallel (a) and perpendicular (b) polarization. Since the complementary structure has only one absorption dip, the phase shift curve does not have regions which produce positive delay. Thus, for the complementary structure, slow light phenomena do not occur well. However, sharp negative time delay is observed for the corresponding absorption window.

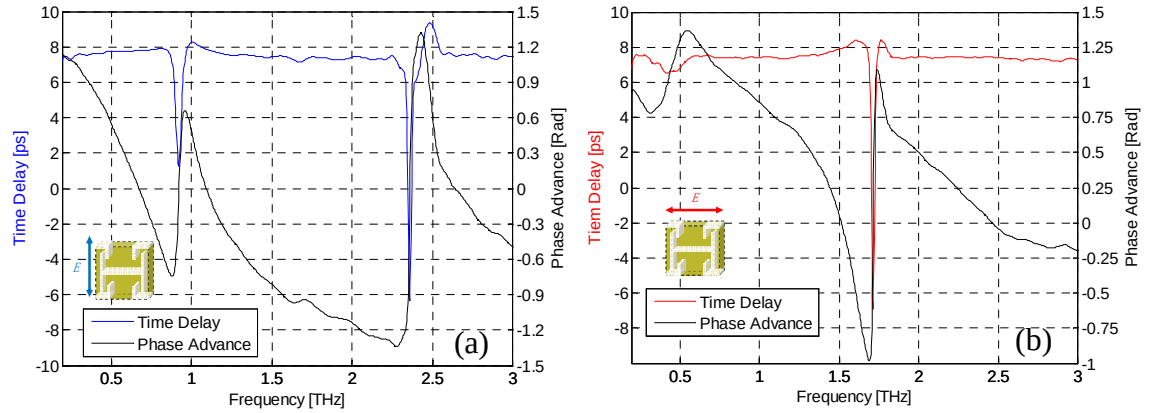

Figure 4-8 Measured time delay and phase advance of complementary fractal H on silicon wafer: (a) Parallel and (b) Perpendicular. For parallel polarization, dip at 0.92 THz: time delay = 1.24 ps, dip at 2.48 THz: time delay = -6.24 ps, and peak at 2.48 THz:

time delay = 9.45 ps. For perpendicular polarization, hill at 1.61 THz: time delay = 8.47 ps, dip at 1.71 THz: time delay = -6.92 ps, and hill at 1.77 THz: time delay = 8.44 ps.

4.4 Summary

In conclusion, we experimentally demonstrated time delay of the complementary fractal metamaterial. Its phase advance showed extreme dispersion. However, it does not include negative dispersion which produces positive time delay. Instead, fast light was observed within the range of positive dispersion. Thus, the complementary structure is not suitable for slow light device.

CHAPTER V

HIGH SPECTRAL RESOLUTION OF SLOW LIGHT MEASUREMENT

5.1 Introduction

In this chapter, we investigate the fractal metamaterial structure on Mylar, a Polyester film, as a substrate instead of silicon wafer. Again, a phase dispersion is the extremely important factor for the slow light characterization. Since such dispersion occurs in extremely short frequency range, measurement with higher spectral resolution is definitely needed. I will show background and problem that previous measurement has from section 5.1.1. Then a new technique to enable much longer time domain scan and to obtain accurate slow light analysis will be shown from section 5.1.2. Before I start next section, I would like to recite the Eq. (1-21):

$$t_g(\omega) = -\frac{\delta\phi(\omega)}{\delta\omega}. \tag{1-21}$$

Measurement of time delay requests accurate phase and frequency change in very short frequency range.

5.1.1 Spectral Resolution of Silicon

Figure 5-1(a) shows time domain signal of blank silicon wafer (640 nm think, n-type resistivity 12 Ω cm). The total scan time is 66.7 ps. According to Eq. (2-1), the scanning step Δt is 0.033 ps (total scanning points = 2000). The reflections due to the second surface of silicon come every ~ 14.5 ps after the first transmitted beam. The corresponding Fourier transformed amplitude spectrum and phase advance are illustrated in Figs. 5-1(b) and (c), respectively. These reflections in the time domain signal spoil the spectrum and the accuracy is lost. In the investigation of a structure on Si wafer, we normally set the total scan time of 17.1 ps (each step ≈ 0.033 ps, total sampling point = 512) to avoid the reflections. Therefore, from Eq. (2-17), the spectral resolution is [34]

$$\Delta f_{\text{Si wafer}} = \frac{1}{512 \times \frac{2 \times 5 \times 10^{-6} m}{2.998 \times 10^{8} m/s}} \approx 59.2 \text{ GHz}. \quad (5\text{-}1)$$

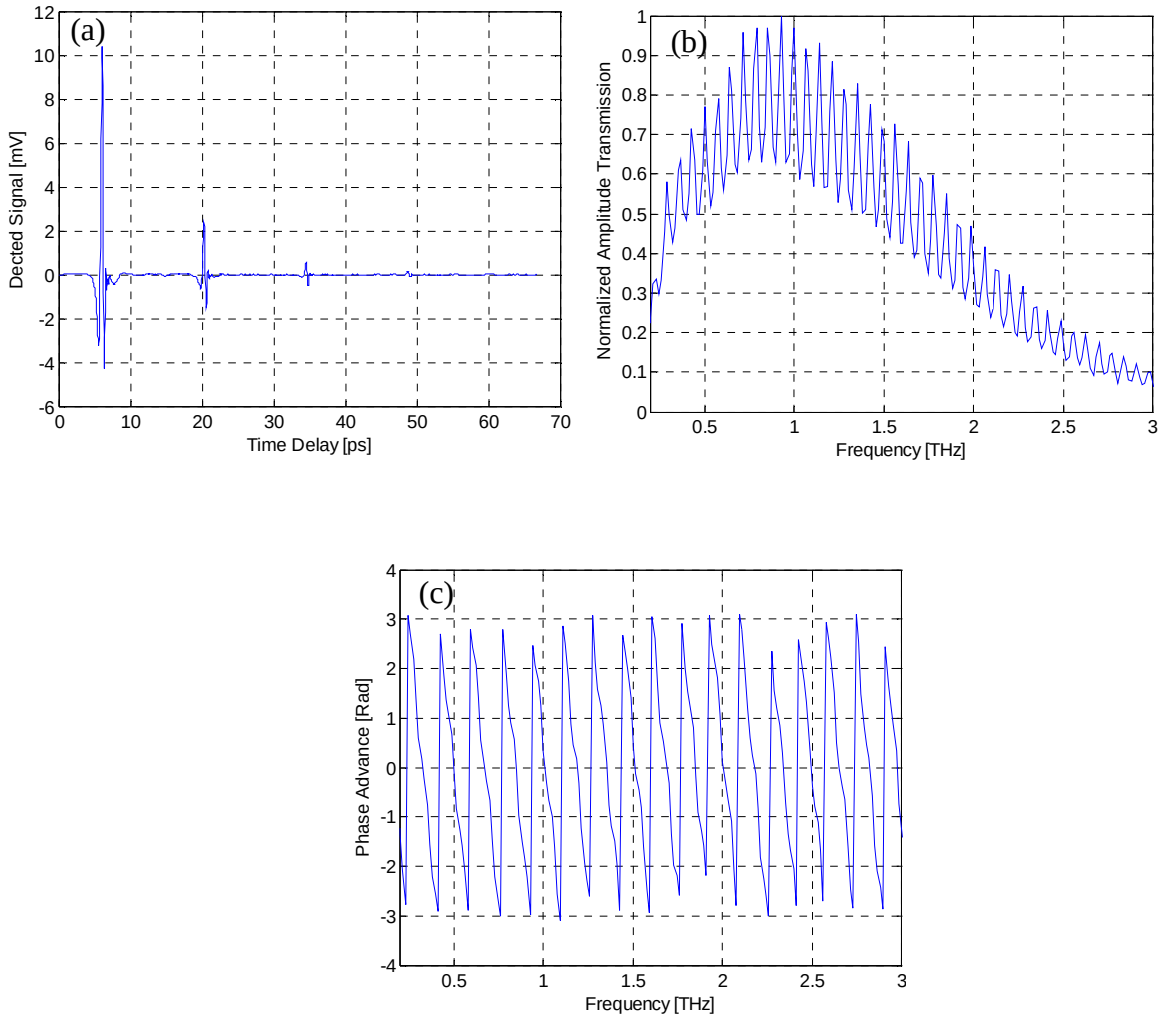

Figure 5-1 Measured electric pulse of blank Si wafer: (a) Time domain signal, (b) Frequency domain spectrum, and (c) Phase advance. Total sampling points = 2000, and total scan time is 66.7 ps. The function "unwrap" is not applied to the phase curve.

Zero padding consists of adding zeros to a time domain signal when it is converging zero. Using zero padding often makes its result reasonable. This function does not have negative impact on the basic characterization of metamaterial, such as peak position, phase shit and some indexes unless their change is not very rapid in short frequency range. For the EIT characterization, however, zero padding is not a recommendatory solution. Fig. 5-2(a) shows the transmission spectra of the positive fractal H structure used in chapter 4. In Figs. 5-2(b) and (c), its phase shift and time delay curves are shown. Black solid curve is the original data. For the red solid curve, 3488 zeros have been added after the time domain signal so that the total points are 4000. The spectral resolution is [34]

$$\Delta f_{\text{Zero Padding}} = \frac{1}{4000 \times \frac{2 \times 5 \times 10^{-6} m}{2.998 \times 10^{8} m/s}} \approx 7.58 \text{ GHz}. \quad (5\text{-}2)$$

Though, zero padding produces more reasonable data, it cannot not solve the essential problem that measurement of silicon wafer has. To increase the accuracy of the measurement of rapid change in very short frequency range, such as extreme dispersion, we definitely need to find a whole new measurement technique to obtain more accurate properties.

A thick wafer can solve this problem by extending time domain scan length. However, some intractable defects still remain. First, the thick wafers are very expensive. Next is that it is not suitable for the device to be heavy and takes up room. Light, portable, and inexpensive devices are definitely requested.

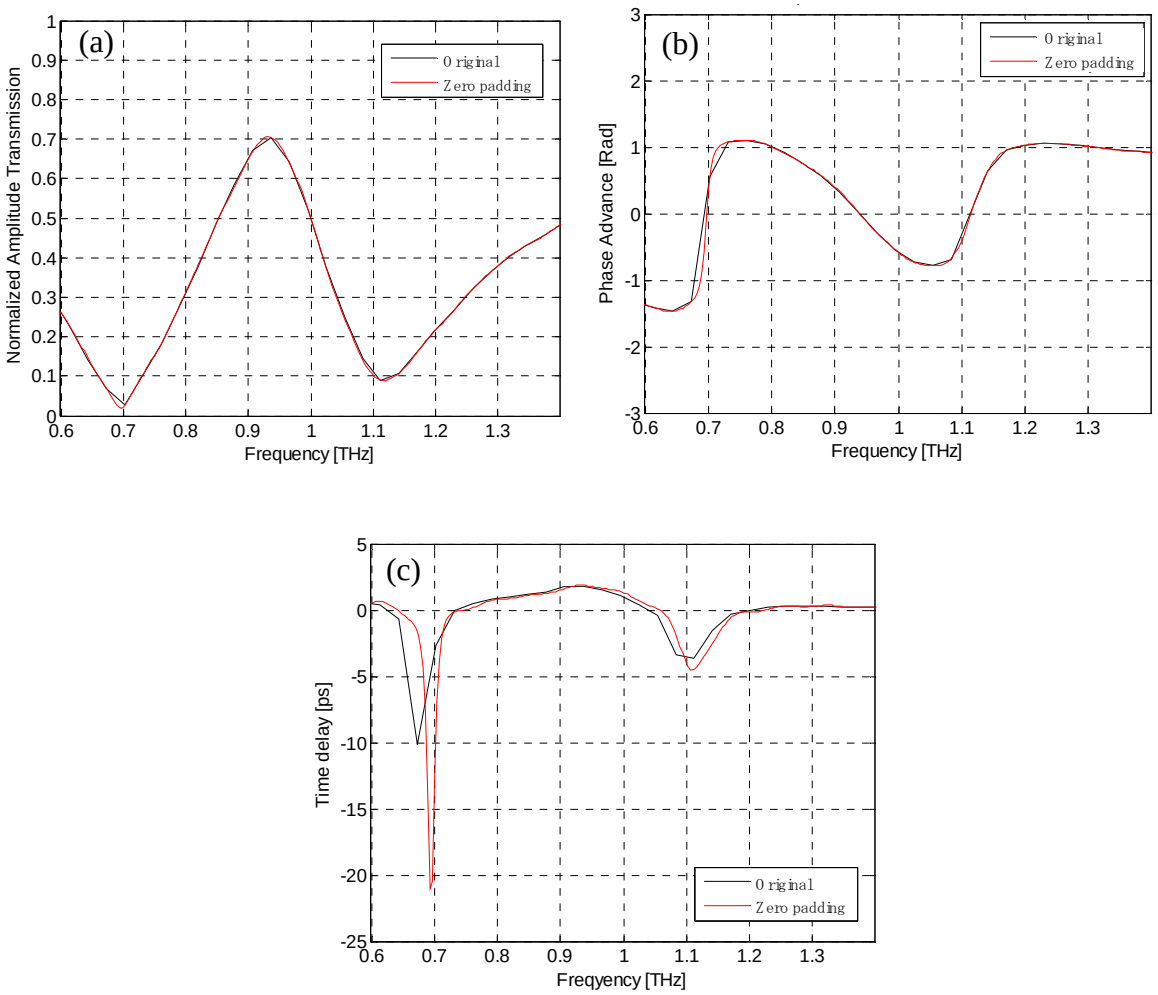

Figure 5-2 Comparison of short scan and zero-padded data: (a) Frequency domain spectra, (b) Phase advance, and (c) Time Delay. The black line is the original data with considering the refection. The red line is the data with zero padding applied.

5.1.2 Spectral resolution of Mylar

Mylar, we used in this experiment, is a commercial polyester film whose thickness and permittivity are 22 μm and 2.8, respectively [46]. Figures 5-4(a) and (b) show pulses transmitted through the film and its frequency domain spectra. The reflection signal is not found in the time domain data since the low refractive index and thin thickness make the reflection negligible. Moreover, its frequency domain spectra show that the absorption is

uniformly small in this frequency region. Thus, structures fabricated on Mylar can be treated as quasi-free standing structure. There is no limitation of scanning time. Mylar allows us to measure it with high spectral resolution which gives more accurate data.

$$\Delta f_{\text{Mylar}} = \frac{1}{(\text{no-limitation}) \times \frac{2 \times 5 \times 10^{-6} m}{2.998 \times 10^{8} m/s}} = (\text{High Resolution}). \quad (5\text{-}3)$$

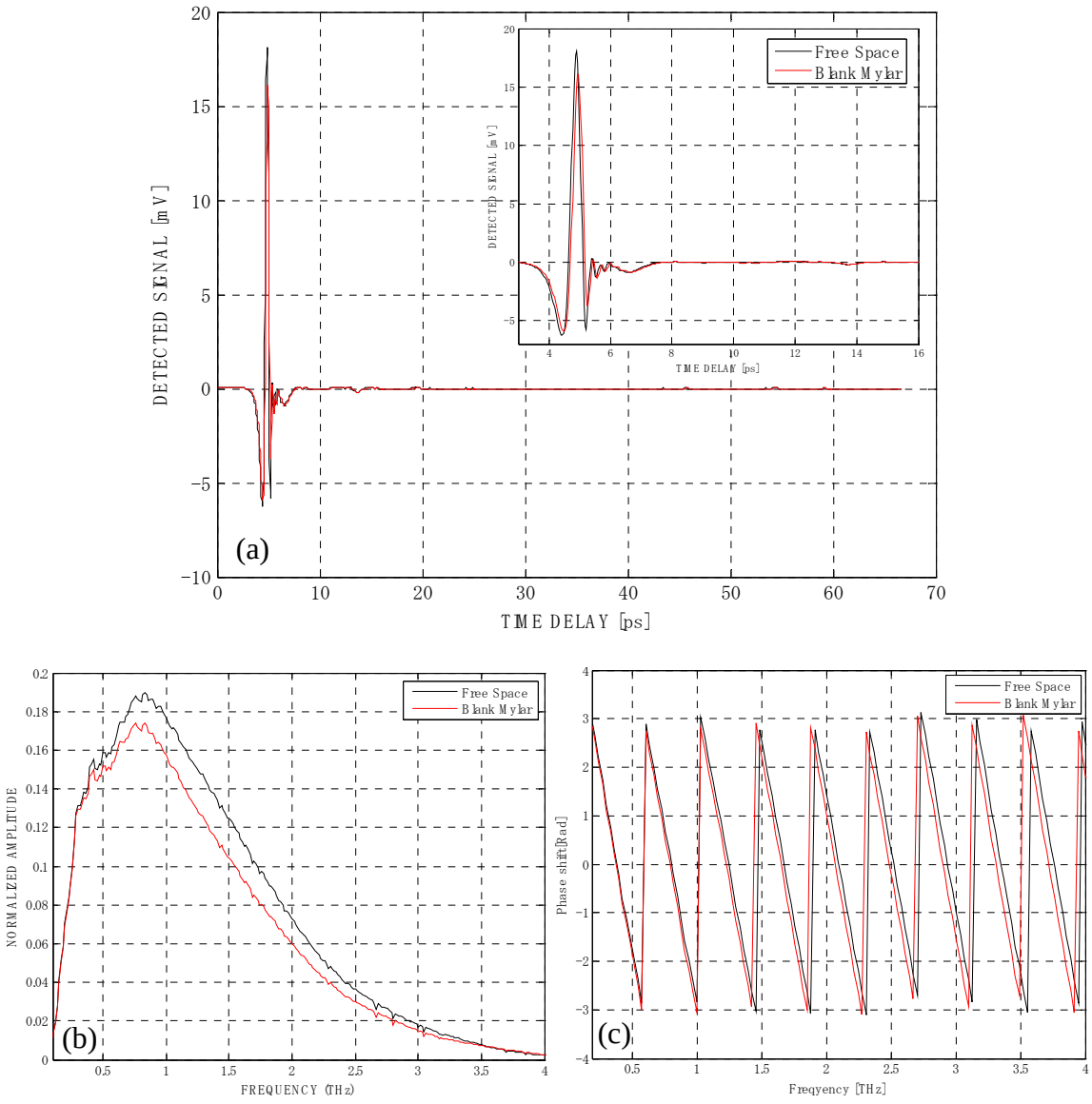

Figure 5-4 Measured spectra of blank Mylar: (a) Time domain spectrum, (b) Frequency domain spectra, and (c) Phase Advance. Total scan time is 66.7 ps (Total sampling points = 2000, and total scan time is 66.7 ps).

5.2 Sample Fabrication and Simulation

Positive type fractal Hs of 200 nm thick Al metal structures are fabricated by conventional photolithography and evaporation technique on Mylar. Dimensions are exactly equal to these of the positive type structure. The dimensions of the larger H are a = 45, b = 48, w_1 = 4, and w_2 = 5 µm. The dimensions of the smaller H are c = 29, d = 28, and w_1 = 4 µm. The periodicity P is 50 µm.

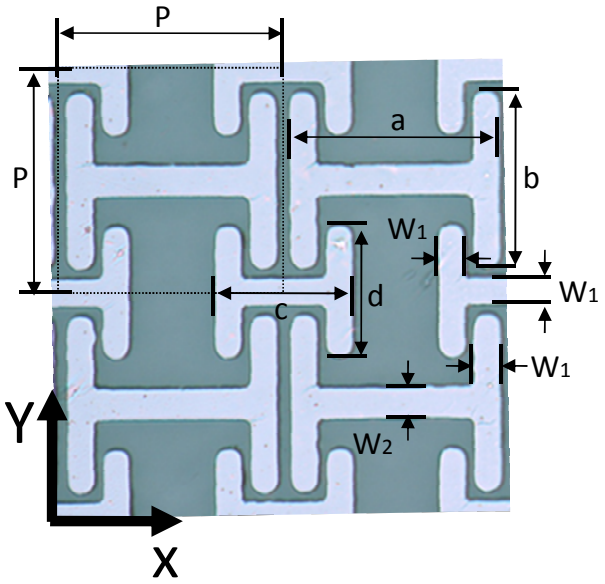

Figure 5-4 Optical image of the fractal H on Mylar: P = 50µm. a = 45, b = 48, c = 29, d = 28, w_1 = 4 and w_2 = 5µm.

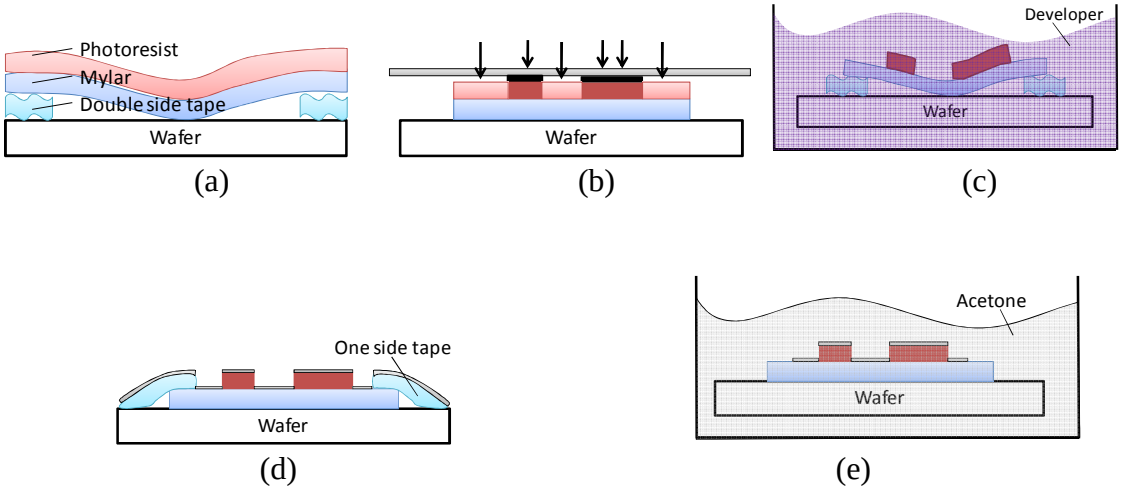

Figure 5-5 Fabrication techniques for Mylar: (a) Photoresist Coating, (b) Exposure, (c) Development, (d) Metalization, and (e) Lift-off.

Delicate and complicated fabrication techniques were required to create structures on Mylar. Some of them are worth to note here, as shown in Fig. 5-5. During the photoresist coating, double side tape was used in order to fix the film on the wafer (Fig. 5-5(a)). Here, the wafer is used as a film stand. Since the film easily collects particles, the surface and space between the wafer and the film are needed to be cleaned with acetone. Photoresist coating and soft bake can be operated as usual. Then, cut off the edge of the film which contain the double side tape and remove the wafer. The film must contact the mask tightly during the exposure (Fig. 5-5(b)). The exposure time is same as that for silicon wafer. Before development, one should use the double side tape again to fix the film on the substrate to avoid that the solvent destroys the structure in case the film is curved or vibrated strongly (Fig. 5-5(c)). Use twister to hold the wafer and swing it in the solvent. If a small amount of photoresist remains on the surface, it MUST fail during the lift off process after evaporation. Before the metallization, fix the film and wafer by using one side tape to make the surface smooth (Fig. 5-5(d)).

During thermal metallization, one needs to increase the current slower than usual to form the metal film slowly. In the lift-off process, it is better to mount the film on a wafer WITHOUT tape and put into the solvent. This prevents that strong inflection applies to the film (Fig. 5-5(e)). Lift-off process has difference depending on the type photoresist used in the beginning. For positive resist, such as S1813 or PA1-4000A, leave it in the acetone more than 10 min, and then apply the ultra sonic bath very carefully. If the excess metal surface is not removed even after one hour later, the sample is defective. After the lift-off, bring the Mylar sample into the clean room and wash the surface with acetone. Then it can be dried out WITHOUT washing with DI water. For negative resist, such as NR71-3000P, sample needs to go directly into clean room after metallization. A petri dish filled with RR4 is prepared. Then the sample is put in the dish and the lift off process need to be monitored under the microscope. Seven minutes later, the sample can be taken off and washed with DI water. Finally, it is blown dry with compressed air.

Fig. 5-6 shows the simulated amplitude transmission for electric field parallel (a) and perpendicular (b) to the x-axis. The “Larger H” or “Smaller H” means the respective oscillator. Transmission windows for both polarizations become broader compared to that of silicon. For parallel polarization, both larger and smaller H support dipole resonances and each lowest eigenmode is 1.22 and 1.85 THz, respectively. At 1.61 THz, both oscillators are in strong resonance. For electric field parallel to y-axis, similarly, the larger and smaller H support dipole resonances with lowest eigenmodes of 2.81 and 3.80 THz, respectively. For this polarization, the interference effect also dominates over it when both resonators are in

the strong resonance at 3.42 THz. In the phase advance (Fig. 5-6(c)), dispersions are created for both polarizations although their advances are not as large as these of silicon.

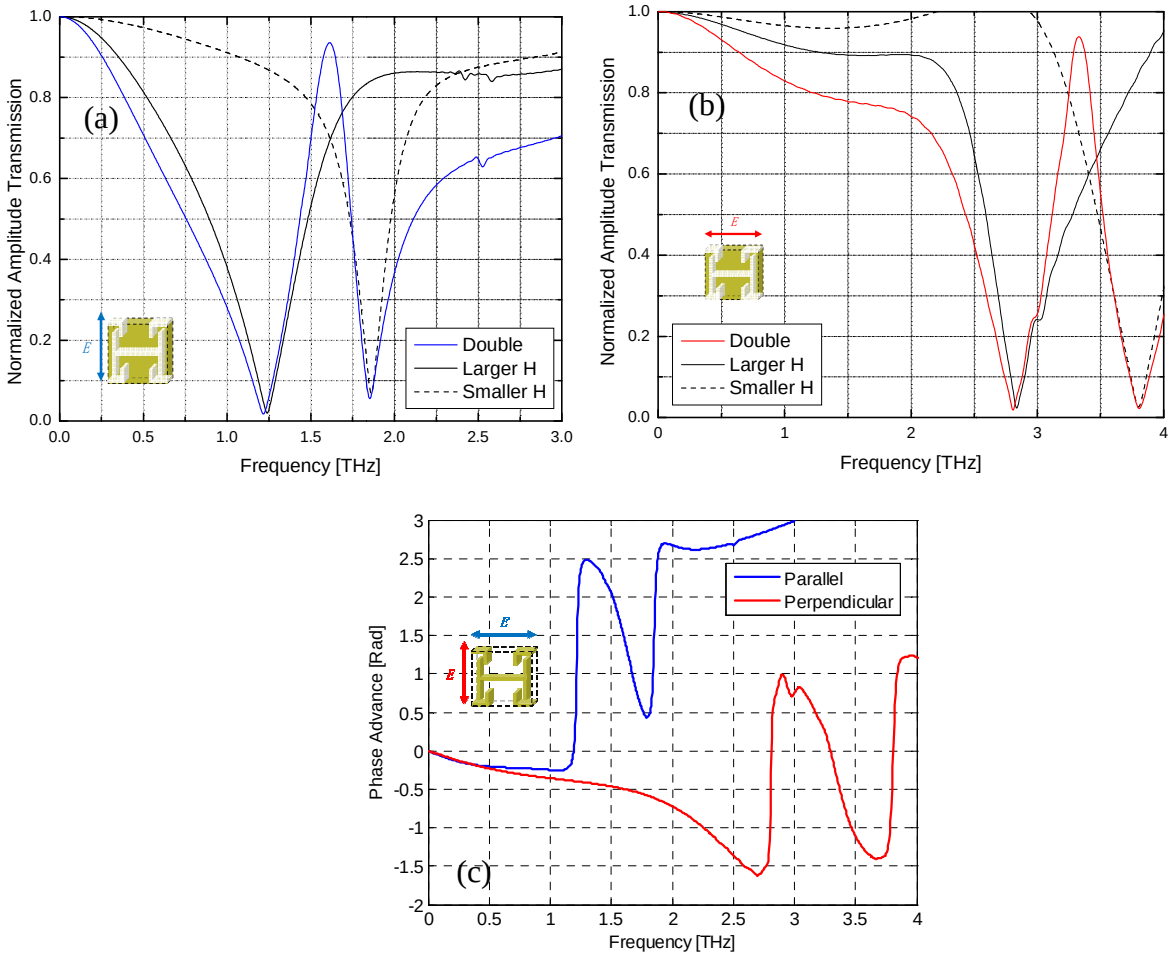

Figure 5-6 Simulated spectra of positive fractal H on Mylar: (a) Parallel, (b) Perpendicular and (c) Phase advance. For parallel polarization, peak at 1.61 THz: FWHM = 0.44 THz and Q = 4.9. For perpendicular polarization, peak at 3.42 THz: FWHM = 0.44 THz and Q = 7.7.

For Mylar, similar approximation used for Eqs. (4-3) and (4-4) can be applied. As one modification, we consider the average effect of Mylar substrate and free space since the Mylar is sufficiently thin.

$$f_{rx_{Mylar}} \approx \frac{c}{2\times 1.84L}\left(\frac{\varepsilon_{d_{Mylar}}+\varepsilon_{d_{air}}}{2}\right)^{-\frac{1}{2}} + a, \qquad \text{for E // X} \qquad (5\text{-}4)$$

$$f_{ry_{Mylar}} \approx \frac{c}{2L}\left(\frac{\varepsilon_{d_{Mylar}}+\varepsilon_{d_{air}}}{2}\right)^{-\frac{1}{2}} + b, \qquad \text{for E // Y} \qquad (5\text{-}5)$$

For x polarization, the constant a is approximately equal to -0.2 THz. For y polarization, the constant b is approximately equal to -0.15 THz. These curves are shown in Figs. 5-7(a) and (b) respectively.

At the same time, the same simulation which was carried out in chapter 4 was carried out for the Mylar structure as well. Again, in this simulation, lengths of resonators and periodicity are uniformly reduced or extended from ΔL = -5 to 35 μm although width w_1 and w_2 are kept as initial values, as shown in Fig. 3-8. Then the characteristics, such as variations of the transmission window and the bandwidth, are investigated. Fig. 3-8 is shown below again for understandability.

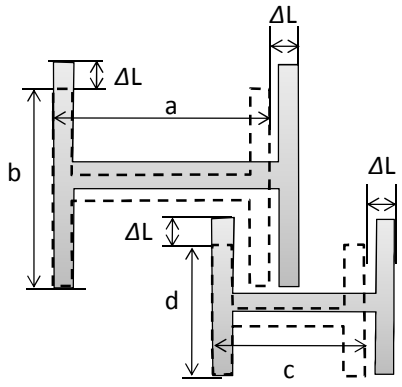

Figure 3-8 Increase the periodicity and lengths: The structures described with dashed lines are original scales. In the simulation, ΔL is extended from -5 to 35 μm with every 5 μm step.

The result is shown in Figs. 5-7 (a) and (b) as well. Since the dielectric constant of Mylar (ε_r = 2.8 at 1 GHz) [46] is much smaller than that of Si (ε_r = 11.3 at 0.1 THz) [40], this causes their electromagnetic behavior, such as the shift of the frequency domain spectra to higher frequency and the broader bandwidth. This result suggests that when we use a metamaterial whose dimensions are exactly same on different kinds of substrates, a substrate with higher permittivity shows narrower transmission window placed in the lower frequency region. Jean-Michel le Floch et al. reported that using higher permittivity materials of larger intrinsic dielectric losses enables better Q-factor [47,48]. This simulation results not only agree with those works, but shows how to conquer the problem that Mylar has. As a consequence, there is a trade off for use of substrate with different permittivity. The silicon substrate allows us to obtain a narrow transmission window placed at lower frequency region but its spectral resolution is low because of the reflection. On the other hand, Mylar allows us high spectral resolution measurement but the transmission window is broad and placed at higher frequency region. To obtain same frequency properties as silicon by using Mylar, we can expand the length of the resonator approximately twice as long as that of silicon. As a result, narrow transmission window and high spectral resolution measurement can be operated by using Mylar.

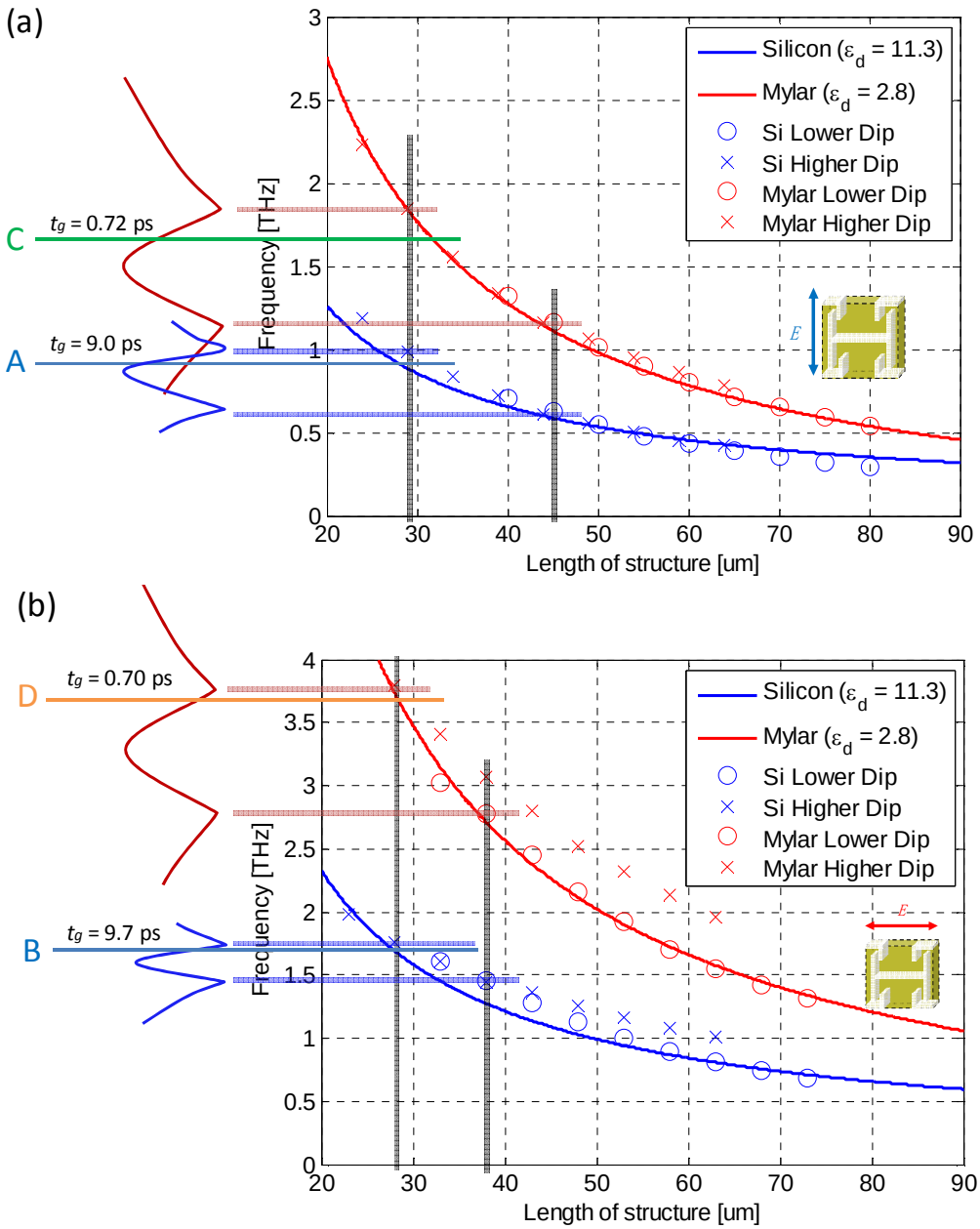

Figure 5-7 Resonant frequency dependence on the structure length. (a) Parallel and (b) Perpendicular polarization. Red and blue solid lines are obtained from equations (4-3) and (4-4). The circle and cross markers are obtained by the simulations based on Fig. 4-10. "Lower Dip" and "Higher Dip" suggest the spectral position of left and right edges of the transmission window, respectively. The gray lines in (a) and (b) are length of the original two resonators for x and y polarization, respectively. A, C and B, D are measured central frequencies of parallel and perpendicular polarizations, respectively.

Figures 5-8(a) and (b) show length dependence of amplitude transmission and frequency for parallel and perpendicular polarizations, respectively. As the length increases, the bandwidth becomes narrow for parallel polarization. Strong dispersion can be expected in these transmission windows. For perpendicular polarization, however, bandwidth gets broad since curves of the lower and higher dip obey two different approximation curves. Also, it worth to recite that sharp peak does not directly mean strong phase change. Numerical salutation is required to make sure that a structure satisfies these formulas and has strong dispersion.

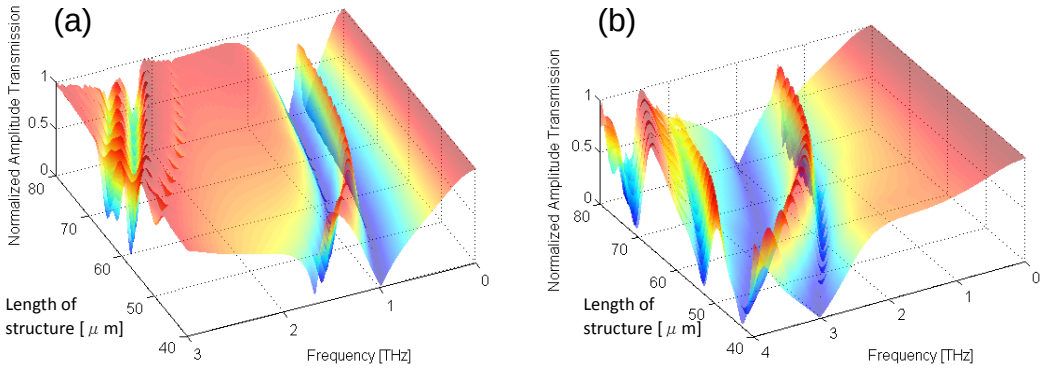

Figure 5-8 Structure length dependence of transmission: (a) Parallel and (b) Perpendicular polarization.

Figure 5-9 shows the total phase change due to the negative dispersion. The total phase changes clearly depend on the permittivity and/or thickness of the substrate. Expanding the resonator to obtain large phase change works more effective when substrate with larger permittivity is used.

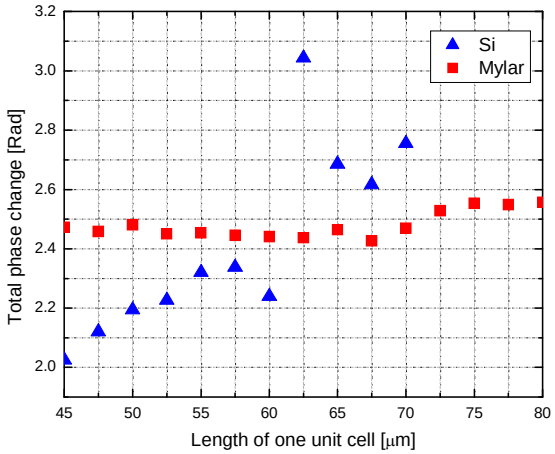

Figure 5-9 Total phase change dependence on the length of one unit cell for parallel polarization.

5.3 Experimental Result and Discussion

Figures 5-10(a) and (b) show measured electric pulse of the fractal H structure on Mylar for electric field parallel and perpendicular to the x-axis, respectively. Compared to the signals obtained from those with silicon substrate, the decay is much steeper. Therefore, the exponential fitting is roughly applied to the signal to compare with that of silicon. Fig. 5-12 shows normalized amplitude transmission (a) and phase advance (b). These curves are obtained without applying zero padding (original). For (a), a broad transmission window is observed around 1.65 THz. For (b), the transmission window occurs at 3.64 THz, almost out of range of our experimental system. The frequency spectrum contains noise like oscillations when it goes higher frequencies. The reflection might affect on them. The Q factors at each resonance are 4.2 and 5.9 for electric field parallel and perpendicular to the x-axis, respectively. Phase change $\delta\phi$ is 1.67 and 1.45 rad for parallel and perpendicular polarization, respectively. They are similar to these of silicon. This agrees with the Delay-Bandwidth Product (DBP) described in Eq. (2-16).

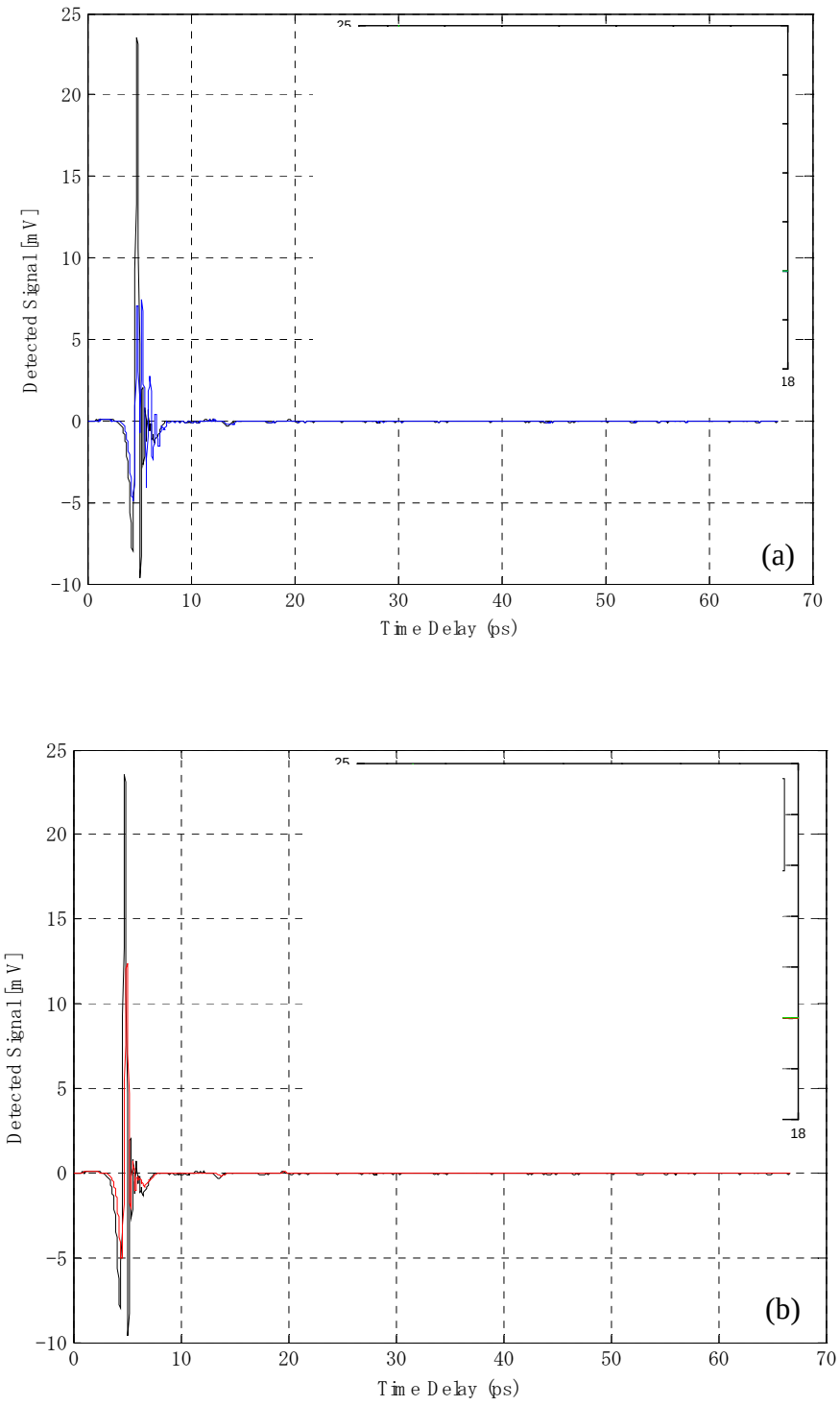

Figure 5-10 Measured electrical pulse for fractal H on Mylar: (a) Parallel and (b) Perpendicular polarization.

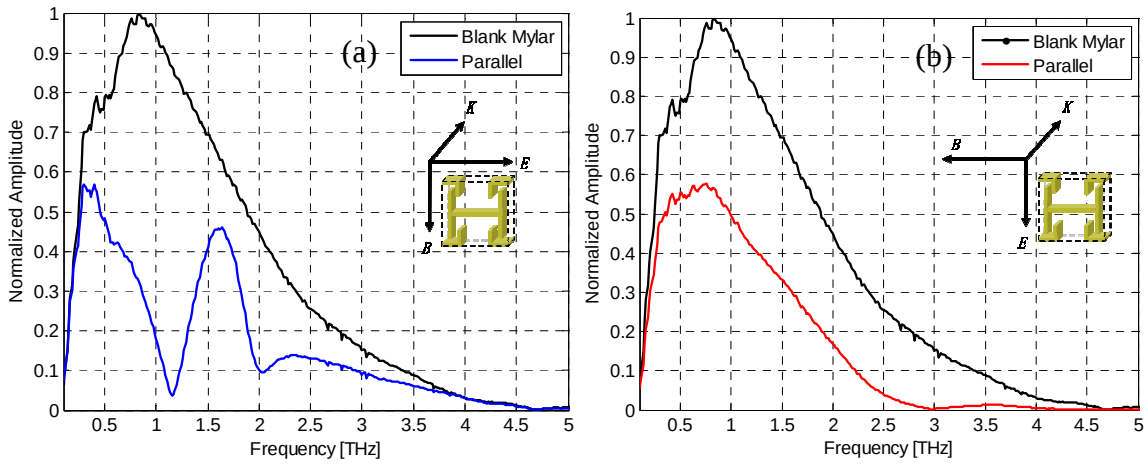

Figure 5-11 Measured frequency spectra of positive fractal H on Mylar: (a) Parallel and (b) Perpendicular polarization.

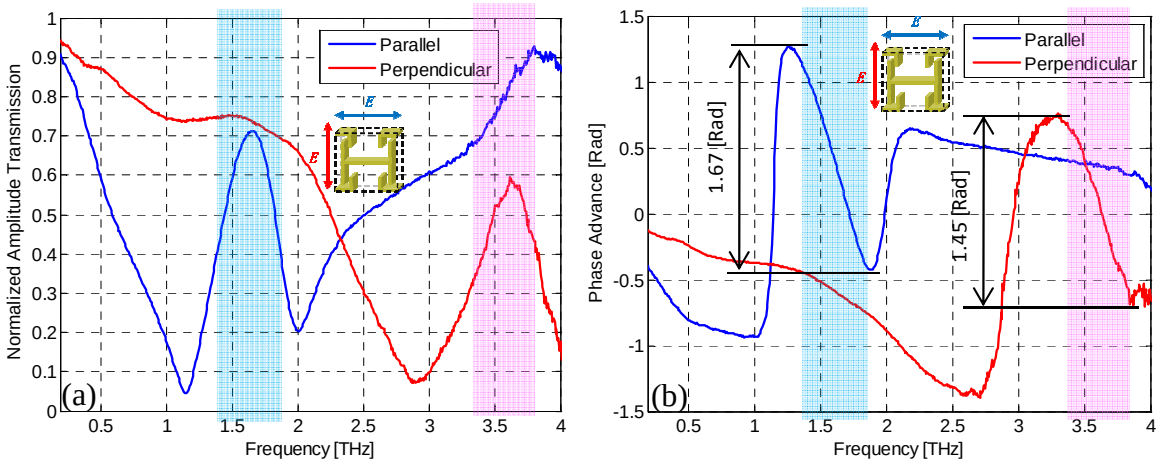

Figure 5-12 Measured normalized amplitude and phase on positive fractal H on Mylar: (a) Normalized amplitude transmission and (b) Phase advance. For parallel polarization, peak at 1.64 THz: FWHM = 0.52 THz and Q =4.2. For perpendicular polarization, peak at 4.70 THz: FWHM = 0.64 THz and Q=5.9. Blue and red colored region correspond to negative phase dispersions.

There is relationship between time delay and decay time. The damping ratio ζ and the exponential attenuation rate α of an under damped resonator can be expressed as

$$\zeta = \frac{1}{2Q} = \frac{\alpha}{\omega_0}, \tag{5-6}$$

$$Q = \frac{1}{2\zeta} = \frac{\omega_0}{2\alpha}, \tag{5-7}$$

where ω_0 is the resonance frequency[49,50].

Relationship between Q factor and time delay can be expressed in one formula:

$$Q = -\frac{\omega_0}{\delta\phi} t_g. \tag{2-15}$$

By substituting Eq. (2-15) into Eq. (5-7), attenuation rate α can be expressed as

$$\alpha = -\frac{\delta\phi}{2t_g}. \tag{5-9}$$

Since $\delta\phi$ is approximately constant, this formula describes that larger time delay produces low attenuation and longer decay time. Since the measured Q factors of Mylar structure are lower than these of silicon, attenuation rate α or decay time is faster than that of silicon. For polarization parallel to the x-axis, the decay time for the Mylar structure is 0.62 ps although it is 1.65 ps for that of silicon. Same result can be seen for perpendicular polarization. As consequence, to obtain larger time delay, the Q factor is needed to be large.

Figure 5-13 shows the time delay and phase advance of the positive fractal H pattern on Mylar. In (a), for electric field parallel to the x-axis, the maximum time delay in that region is 0.71 ps (the velocity of light ≈ 0.51×10^8 m/s). Since it takes approximately 0.12 ps to pass through blank Mylar, this is relatively 0.58 ps slower. Moreover, its signal to noise ratio is very high compared to the result of silicon. For the perpendicular polarization, the maximum

delay is 0.6 ps (the velocity of light ≈ 0.61×10^8 m/s). However, since the transmission window is placed around 4.70 THz, amplitude of transmitted wave is really weak. Moreover, the reflection component effects on these higher frequency region. This is the reason the curve of time delay is noisy. At 1.64 and 1.99 THz for parallel polarization and at 2.87 THz for perpendicular polarization, negative time delay is observed.

In fact, since negative dispersion is not so rapid, those time delays are not remarkable values. From this experiment, however, we found that how dielectric constant of substrate affects the peak position and bandwidth.

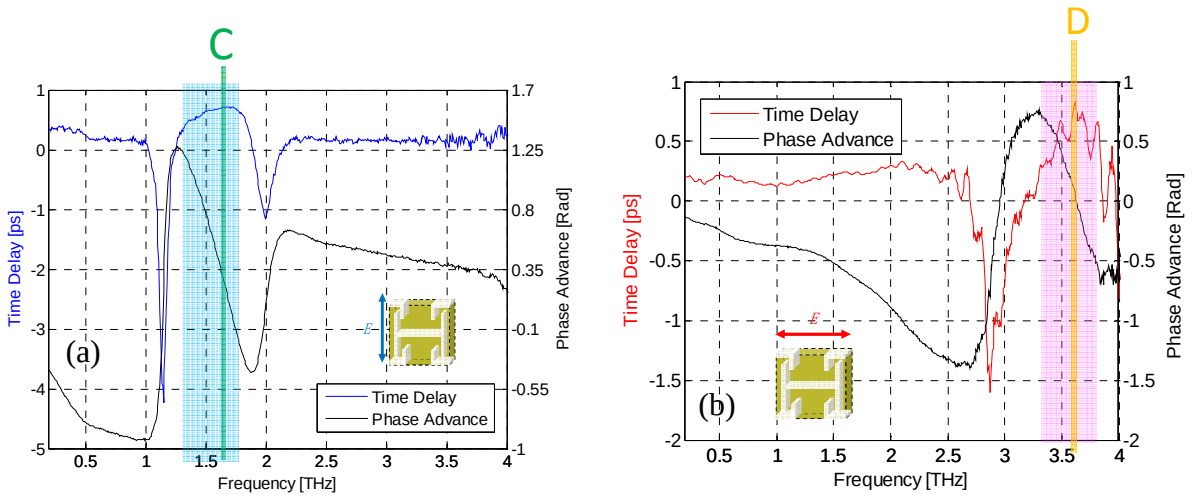

Figure 5-13 Measured time delay and phase advance: (a) Parallel and (b) Perpendicular polarization.

For parallel polarization, dip at 1.15 THz; time delay = -4.25 ps
hill at 1.64 THz; time delay = 0.72 ps (Solid line C)
dip at 1.99 THz; time delay = -1.16 ps
For perpendicular polarization, dip at 2.87 THz; time delay = -1.60 ps
Peak at 4.70 THz; time delay = 0.70 ps (Solid line D)
Blue and red colored region correspond to negative phase dispersions

5.4 Summary

In conclusion, Mylar enable as quaci-free standing metamaterial structure. Increasing the accuracy of time delay has been a challenge because use of silicon wafer has strong reflection after about 15 ps time scan. We achieved high-spectral resolution measurement and obtained accurate time delay. However, with the same fractal H structure and same dimensions as being used on silicon, the measured delay was not remarkably slow. Since permittivity of Mylar is small compared to that of silicon, this created the shift of transmission window, the broad bandwidth, and the dull phase shift which decreases the time delay. From the simulation, we learned that increasing the length of resonators could conquer these problems. Strong dispersion can be expected in the transmission window.

CHAPTER VI

FUTURE WORK

6.1 Inproved slow light device

In this section, I would like to show a design based on the previous experimental results. Fig. 6-1(a) shows the dimensions of the new pattern with P = 100, a = 90, b = 78, c = 65, d = 76, w_1 = 4 and w_2 = 5 μm. The lengths of each resonator are not just simply expanded, but adjusted so that it produces high performance as a slow light device. When this structure is fabricated on Mylar, the simulated transmission and phase are shown in Figs. 6-1(b) and (c), respectively. Much narrower bandwidth and more extreme phase dispersion are achieved. Large time delay can be expected. The advantage of this structure is not only mimicking EIT remarkably, but having multiple transmission windows for both polarizations.

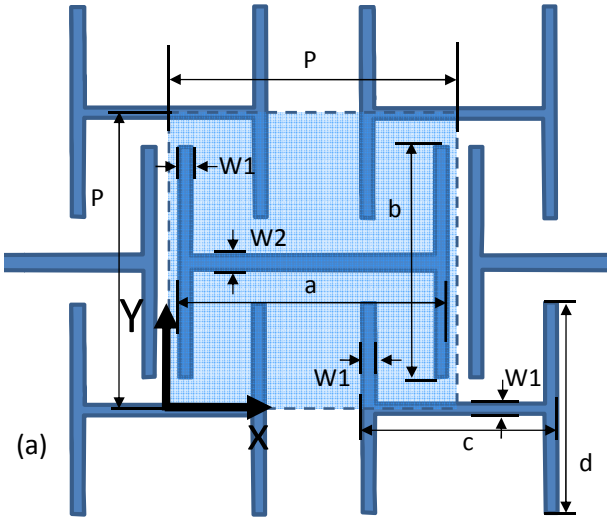

P = 100, a = 90, b = 78, c = 65, d = 76, w_1 = 4 and w_2 = 5 µm.
This structure is fabricated on Mylar.

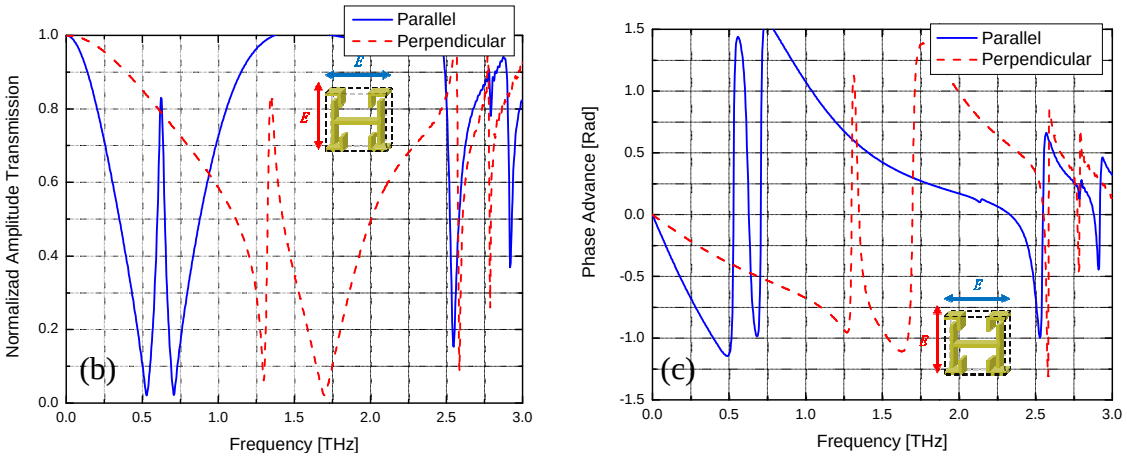

Figure 6-1 Design of metamaterial with narrow bandwidth and extreme dispersion:
(a) Design, (b) Normalized amplitude transmission, and (c) Phase advance. For parallel polarization, peak at 0.62 THz: FWHM = 0.06 THz and Q = 10. For perpendicular polarization, peak at 1.34 THz: FWHM = 0.13 THz and Q = 11.

6.2 Multiple Mylar layers

Metamaterials fabricated on multi-layers are also an interesting topic. As we have seen, the single Mylar metamaterial can be assumed as a quasi-free standing structure. In this section, the characteristics of multiple blank-Mylar films are experimentally characterized. In the measurement, a holder is used to have tightly contacted films. Figs. 6-2(a) and (b) show the time domain data of multiple blank-Mylar films. Fig. 6-3(a) and (b) show the corresponding frequency domain and phase spectra, respectively. For the phase, curves are flipped periodically since their measurement range is $-\frac{\pi}{2} \leq \theta \leq \frac{\pi}{2}$. I did not use function "unwrap" because of the view-ability. The total scanning time and spectrum resolution are 66.7 ps and 15.2 GHz. These time domain signals resemble each other very much and reflection-like signal is not found clearly. In the frequency domain, curves of two and three layers show small-inconsistent characters. However, the low attenuations and unremarkable phase shifts indicate that the multiple layers can also be used for quasi-free standing structures.

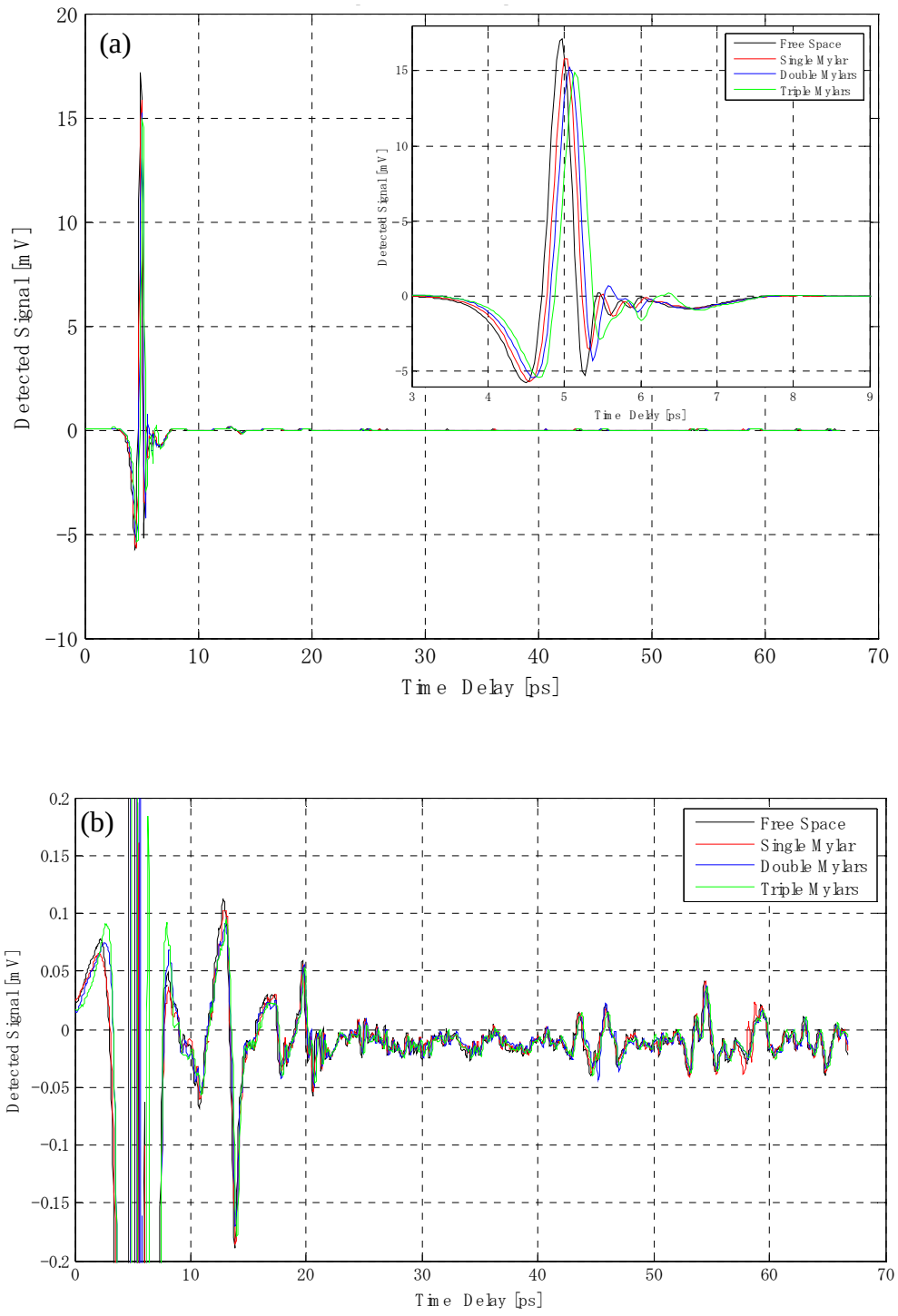

Figure 6-2 Measured time domain data of multiple blank Mylar films: (a) Normal view and (b) Enlarged view.

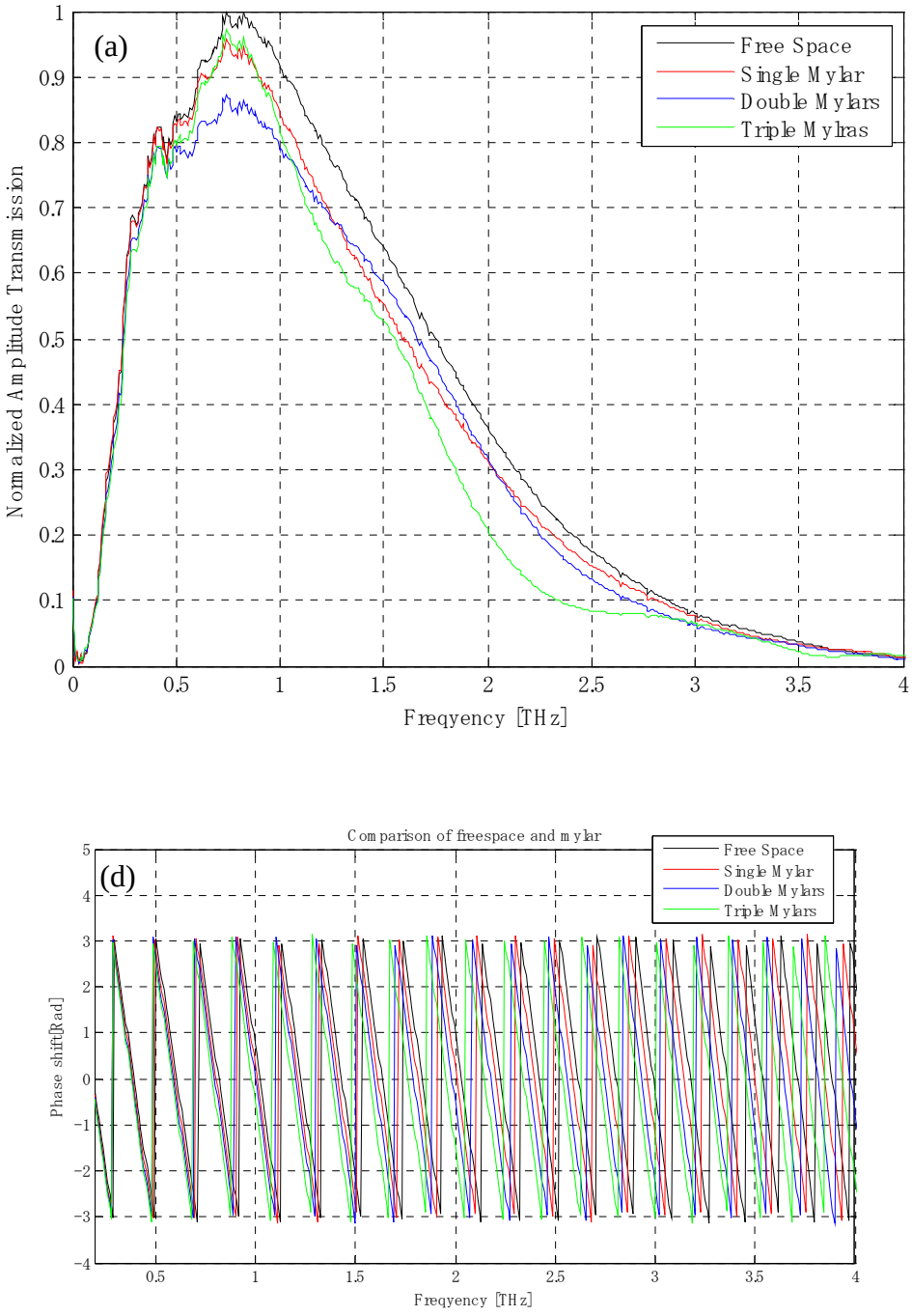

Figure 6-3 Measured frequency spectra and phase advance of multiple blank Mylar films: (a) frequency spectrum and (b) phase advance. The function "unwrap" is not applied to emphasis on the view-ability.

Fabricating slow light metamaterials on multiple mylar layers potentially act more effective slow light device. Fig. 6-4 shows the diagram of beam passing through two slow light layers, A and B. From the chapter 2, the incident beam $x(t)$ and the transmitted signal $y(t)$ through the slow light device A which has the transfer function of $H(j\omega)$ are expressed as [18]

$$x(t) = e^{j\omega t}, \tag{1-16}$$

$$y(t) = |H(j\omega)|e^{j(\omega t+\phi(\omega))}. \tag{1-17}$$

Here, we put another slow light layer B after A. Assume $z(t)$ is the output signal from the layer B. The time profile of $z(t)$and eventual time delay $t_{g_z}(\omega)$ are describes as [18]

$$\begin{aligned} z(t) &= H(j\omega)y(t) \\ &= |H(j\omega)|e^{j\phi(\omega)}|H(j\omega)|e^{j(\omega t+\phi(\omega))} \\ &= |H(j\omega)|^2 e^{j(\omega t+2\phi(\omega))}, \end{aligned} \tag{6-1}$$

$$t_{g_z}(\omega) = 2\mathrm{t_g}(\omega). \tag{6-2}$$

where $\mathrm{t_g}(\omega)$ is the time delay created by the first layer. As a consequence, the phase change and the time delay are proportional to the number of layers.

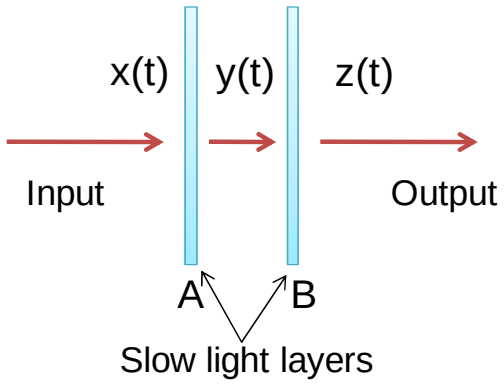

Figure 6-4 Diagram of light passing through two slow light layers.

However, if those layers are placed enough close each other, multiple reflection due to these surfaces interfere. As a result, they potentially act like Fabry-Pérot interferometer and the output signals are decided due to the space between layers [15,51]. To prevent this, the metamaterials are needed to be fabricated three dimensionally, because our planar metamaterials potentially act like mirror. Or we have to place these layers with appropriate distances each other to make the multiple reflection effect as small as possible.

Investigation of multiple layers brings us new perspective to the study of so called "mechanical matamaterial". By adjusting the position of each layer two-dimensionally, we can learn variety of characteristics with high spectral resolution. N. Papasimakis *et al*. investigated the EIT-like phenomena with the double-layer fish-scale structures on 1.5 mm PCB laminate [25]. They used "trapped mode" resonances to weakly couple to free space. If we can adjust one layer of the fish structures longitudinally, it might tune the frequency position of the transmission window, making a powerful control device.

6.3 Sensing devices

Slow light metamaterials can potentially act as a high sensitive interferometer [46]. Figure 6-5 shows the schematic diagram. An incident beam is divided into two by using a splitter. One of the beams transmits through the normal arm. Properties of signal are not changed and this beam will be used as a reference. Another beam passes through the slow light arm. As a slow light device, metamaterial can be used in it. At the accumulator, by

using interference effect, the properties of information can be obtained with high sensitivity.

There are three benefits:

(1) The pulse passes through the slow light arm with very slow group velocity. The sample contributes to the light for long time.

(2) The light passing through the slow light arm contains strong and approximately linear phase dispersion. A small phase change due to the sample can be detected clearly.

(3) Signals coming from normal and slow light arms interfere and surrounding effects, such as temperature and humidity, can be cancelled.

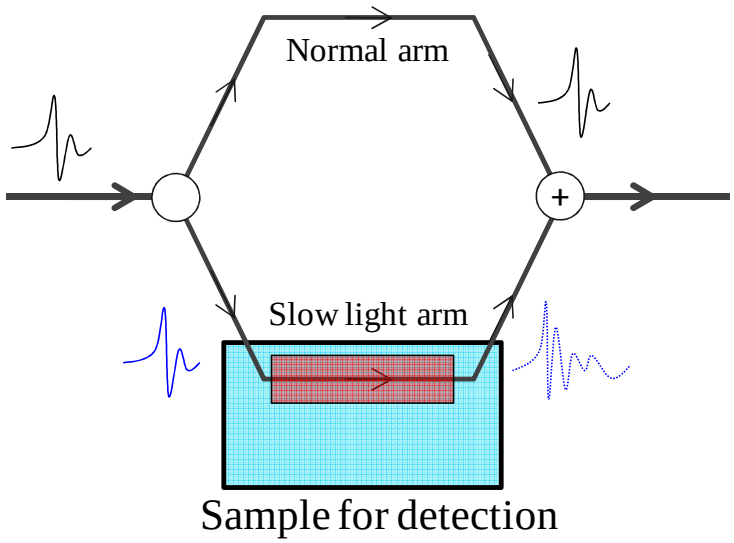

Figure 6-5 Schematic diagram of slow light sensing device. The red colored area contains slow light devises. Sample is filled in the blue colored area.

From the interference theory, the phase difference of interferometer is expressed as

$$\Delta\phi(\upsilon) = \frac{2\pi\upsilon}{c} n(\upsilon) L, \tag{6-2}$$

where $\Delta\phi(\upsilon)$ and $n(\upsilon)$ is the change rate of the phase difference and refractive index of the slow light medium [52]. The sensitivity of the spectral is related to the change rate with the signal frequency υ. The sensitivity of the interferometer is thus expressed as

$$\frac{\Delta\phi(\upsilon)}{d\upsilon} = \frac{d}{d\upsilon}\left(\frac{2\pi\upsilon}{c} n(\upsilon) L\right) = \frac{2\pi L}{c}\left(n + \upsilon\frac{dn}{d\upsilon}\right) = \frac{2\pi L n_g}{c} \tag{6-3}$$

where n_g is group index [52]. Thus, the sensitivity of the sensing device or interferometer relies on effective length of the slow light arm.

Figure 6-6 shows the simple sketch of the amplitude transmission and phase change due to the sample at the slow light arm. The peak position shifts due to the refractive index of the sample (a). Since the group velocity in the transmission window is very slow, the light is contributed from the sample for relatively long time. This enables the very sharp absorption line. The corresponding phase change occurs, as shown in (b). Since the phase of the incident beam has linear properties, small phase change due to the sample can be detected obviously.

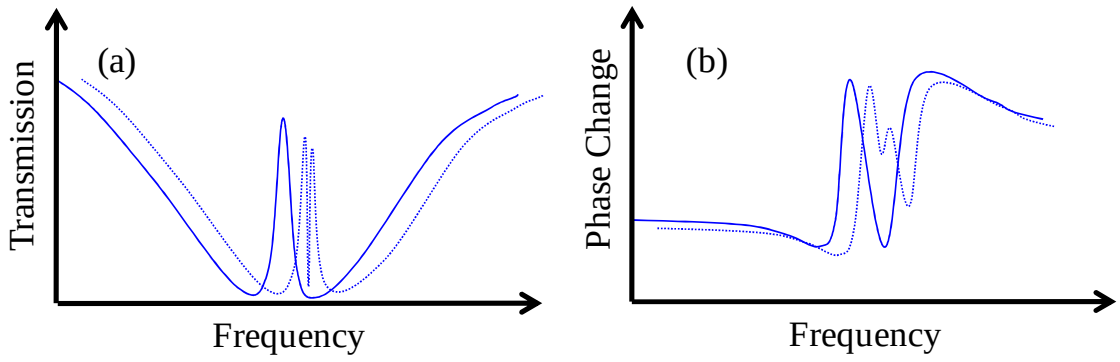

Figure 6-6 Sketch of the amplitude transmission and phase change due to the sample. the solid blue curves are the incident pulse to the sample container. The dashed blue curves are the output from the sample container. (a) and (b) are spectra with slow light devise.

CHAPTER VII

Conclusion

We experimentally demonstrated the slow light effect in the fractal H metamaterial fabricated on silicon. This slow light device produces two transmission-windows for each polarization. Narrow bandwidth and strong-negative phase dispersion are the key factors to produce large time delay. However, the device showed low Q factor and the detected slow light was not remarkable. We could conquer this problem by expanding the lengths of the resonators since this method creates narrow bandwidth. In addition, we need to have a strong phase dispersion as well.

We also experimentally demonstrated time delay of the complementary fractal metamaterial. Its phase advance showed extreme dispersion. However, it does not include negative dispersion which produces positive time delay. The complementary structure is not suitable for slow light device.

Mylar substrate enables quaci-free standing structure. We achieved high-spectral resolution measurement and more accurate time delay compared to that of using of

silicon wafer as substrate. However, when we use fractal H structure with same dimensions used on silicon, the measured delay was not remarkably slow. Since the permittivity of Mylar is small compared to that of silicon, this created the shift of transmission window, the broad bandwidth, and the dull phase shift which produced small delay. There is a trade off for use of substrate with different permittivity. When a metamaterial structure with same dimensions is used as a slow light device, the silicon substrate allows us to obtain a narrow transmission window placed in the lower frequency region but its spectral resolution is low because of the reflection. On the other hand, Mylar enables high spectral resolution measurement but the transmission window is broad and placed at higher frequency region. We can expand the length of the resonator approximately twice as long as that of silicon to obtain slightly similar properties. Strong-negative dispersion can be expected on the metamaterials on Mylar.

REFERENCES

[1] C. Caloz, and T. Itoh, Electromagnetic Metamaterials : Transmission Line Theory and Microwave Applications, Wiley (2008).

[2] Ranjan Singh, PhD Thesis, Engineering the resonance of terhertz metamaterials, (2009).

[3] V. G. Veselago, The Electrodynamics of substances with simultaneously negative values of ε and μ, Soviet Physics Uspekhi, **10**: 509 (1968).

[4] John B. Pendry and David R. Smith, The Quest for the Superlens, Scientific American, **295**: 60-67 (2006).

[5] J. B. Pendry, Negative Refraction Makes a Perfect Lens, Phys. Rev. Lett., **85**: (2000).

[6] R. A. Shelby, D. R. Smith, and S. Schultz, Experimental Verification of a Negative Index of Refraction , Science **292**, 5514, (2001).

[7] D. R. Smith, and N. Kroll, Negative Refractive Index in Left-Handed Materials, Phys. Rev. Lett., **85**, 2933, (2000).

[8] Ranjan Singh, Carsten Rockstuhl, Falk Lederer, and Weili Zhang, The impact of nearest neighbor interaction on the resonances in terahertz metamaterials, **94**: 02116 (2009).

[9] W. J. Padilla, A. J. Taylor, C. Highstrete, Mark Lee, R. D. Averitt, Dynamical Electric and Magnetic Metamaterial Response at Terahertz Frequencies, Phys. Rev. Lett. **96**: 107401 (2006).

[10] Abul K. Azad, Jianming Dai, and Weili Zhang, "transmission properties of terahertz pulses through subwavelength double split-ring resonators", Opt. Soc. Am., **31**: 634 (2006).

[11] D. R. Smith, Willie J. Padilla, D. C. Vier, S. C. Nemat-Nesser, and S. Schultz, Composite Medium with Simultaneously Negative Permeability and permittivity, Phys. Rev. Lett., **84**: 4184 (2000).

[12] Robert W. Boyd, Daniel j. Gauthier, "Slow" and "Fast" Light, (2001).

[13] Daniel J. Gauthier, and Robert W. Boyd, Fast light, Slow light and optical precursors: what does it all mean?, Photonics spectra, 82 (2007).

[14] Eugene Hecht, Optics, Person Addison Wesley (2002).

[15] Keigo Iizuka, Elements of photonics volume I, Wiley-Interscience (2002).

[16] Roqer Penrose, The Road to Reality: A Complete Guide to the Laws of the Universe, Knopf (2004).

[17] wikipedia. org, http://en.wikipedia.org/wiki/Slow_light.

[18] wikipedia. org, http://en.wikipedia.org/wiki/Group_delay_and_phase_delay.

[19] Shlomo Engelberg, Digital Signal Processing: An Experimental Approach, Springer, (2010).

[20] Eugene N. Bruce, Biomedical Signal Processing and Signal Modeling, Wiley-Interscience, 2000.

[21] Applied Radio Labs, "Group Delay Explanations and Applications", (1999).

[22] Nikitas Papasimakis and Nikolay I. Zheludev, Metamaterial-Induced Transparency Sharp Fano Resonance and Slow Light, OPN Optics & Photonics News, 23 (2009).

[23] Stephen E. Harris, Electromagnetically Induced transparency, Physics Today, **50**: 36 (1997).

[24] C. L. Garrido Alzar, M. A. G. Martinez, P. Nussenzveig, "Classical analog of electromagnetically induced transparency", Am. J. Phys. **70**: 37 (2002).

[25] Philippe Tassin, Lei Zhang, Thomas Koschny, E. N. Economu, and C. M. Soukoulis, Planer designs for electromagnetically induced transparency in metamaterials, Opt. Exp. **17**: 5595 (2009).

[26] N. Papasimakis, V. A. Fedotov, and N. I. Zheludev, Metamaterial Analog of Electro magnetically induced transparency, Phys. Rev. Lett. **101**: 253903 (2008).

[27] Sher-Yi Chiam, Ranjan Singh, Carsten Rockstuhl, Falk Lederer, Weili Zhang, and Andrew A. Bettiol, Analogue of electromagnetically induced transparency in a terahertz metamaterial, Phys. Rev. B., **80**: 153103 (2009).

[28] P. Tassin, Lei Zhang, Th. Koschny, E. N. Economou, and C. M. Soukoulis, Low-Loss Metamaterials Based on Classical Electromagnetically Induced Transparency, Phys. Rev. Lett., **102**: 053901 (2009).

[29] Ranjan Singh, Carsten Rockstuhl, Falk, Lederer, and Weili Zhang, Coupling between a dark and a bright eigenmode in a terahertz metamaterial, Phys. Rev. B. **79**: 085111 (2009).

[30] D. Grischowsky and N. Katzenellenbogen, Femtosecond Pluses of Terahertz radiation: Physics and Applications, OSA Proceedings on Picosecond and Optoelectronics, **9**, 9 (1991).

[31] M. van Exter, Ch. Fattinger and D. Grischkowsky, Terahertz Time Domain Spectroscopy of Water Vapor, Opt. Lett., **14**, 1128 (1989).

[32] Jianming Dai, Jiangquan Zhang, Weili Zhang and D. Grischkowsky, THz Time - Domain Spectroscopy Characterization of the far-infrared absorption and index of refraction of high-resitivity, float-zone silicon, J. Opt. Soc. Am. B., **21**: 1379 (2004).

[33] Franc Träger, Lasers and optics, Springer handbook, 1101(2007).

[34] Lecture note of Dr. D. Grischkowsky's course; ECEN5853 Ultrafast Optoelectronics (Fall 2008).

[35] Tae-In Jeon, PhD thesis, New applications of THz Time-domain spectroscopy, (1997).

[36] Yongyao Chen, A report for Ph.D. priminally exam, Using Metallic Micro-structured Devices Manipulating THz waves (2010).

[37] Toshihiko Baba, Takashi Kawasaki, Hirokazu Sasaki, Jun Adachi, and Daisuke Mori, Large delay-bandwidth product and tuning of slow light pulse in photonic crystal coupled waveguide, Opt. Exp., **16**, 9245 (2008).

[38] Peter Jänes, Jonas Tidström, and Lars Thylén, "Limits on Optical Pulse Compression and Delay Bandwidth Product in Electromagnetically Induced Transparency Media", J. of Lightwave Technology, **23**: 3893 (2005).

[39] C. L. Haynes, A. D. Mcfarland, L.Zhao, R. P. Van Duyne, and G. C. Schatz, The Importance of Radiative Dipole Coupling in Two-Dimensional Nanoparticle Arrays, J. Phys. Chem. B **107**, 7337 (2003).

[40] Xinchao Lu, Jiaguang Han, and Weili Zhang, Resonant terahertz reflection of periodic arrays of subwavelength metallic rectangle, App. Phys. Lett., **92**: 121103 (2008).

[41] F. Miyamaru, Y. Saito, M.W. Takeda, B. Hou, L. Liu, W.Wen, and P.Sheng, Terahertz electric response of fractal metamaterial structure, Phys. Rev. B., **77**: 045124 (2008).

[42] T.H. Issac, W. L. Barnes, and E. Hendry, Surface-mode lifetime and the terahertz transmission of subwavelength hole arrays, Phys. Rev. B., **80**: 115423 (2009).

[43] F. Falcone, T. Lopeteg, M. A. G. Laso, J.D. Baena, J. Bonache, M. Beruete, R. Marques, F. Martin, and M. Sorolla, Babinet Principe Applied to the Design of Metasurfaces and Metamaterials, Phys. Rev. Lett., **93**.197401 (2004).

[44] Carsten Rockstuhl, Thomas Zentgraf, Todd P. Meyrath, Harald Giessen, and Falk Lederer, Resonances in complementary metamaterials and nanoapertures, Opt. Exp., **16**: 2080 (2008).

[45] Hou-Tong Chen, John F.O'Hara, Antoinette J. Taylor, Richard D. Averitt, C. Highstrete and Mark Lee, Willie J. Padilla, Complementary planar terahertz metamaterials, Opt. Exp., **15**: 1084 (2007).

[46] S. Krishnamurthy, M. T. Reiten, S. A. Harmon, and R. A. Cheville, Characterization of thin polymer films using terahertz time-domain interferometry, App. Phys. Lett., **79**: 875 (2001).

[47] Jean-Michel le Floch, Michael E. Tobar, Dominique Cros, Jerzy Krupka, Low-loss Materials for high Q-factor Bragg Reflector Resonators, Phys. Lett., **92:** 032901 (2008)

[48] Ranjan Singh, Abul K. Azad, John F. O'Hara, Antoinette J. Taylor, and Weili Zhang, "Effect of metal permittivity on resonant properties of terahertz metamaterials" Opt. Lett., **33**: 1506 (2008).

[49] Rüdiger Paschotta, Encyclopedia of Laser Physics and Technology, Wiley-VCH, (2008)

[50] William McC Siebert, Circuits signals and systems, MIT Press; McGraw-Hill, (1986).

[51] Govind P. Agrawal, Fiber-Optic Communication system, Wiley Inter-Science, (2002).

[52] Zhao Yong, Zhao Huawei, Huang He, Research on high sensitivity optical fiber interference sensing due to slow light, Photonics and Optoelectronics, SOPO 2009.

VITA

SHOICHI ITO

Candidate for the Degree of

Master of Science

Thesis: FRACTAL THZ SLOW LIGHT METAMATERIAL DEVICES

Major Field: Electrical Engineering

Biographical:

Education: Received the Bachelor of Science degree in Electrical and Electric Engineering from Shinshu University, Japan, in December 2008; Completed the requirements for the Master of Science degree in Electrical Engineering at Oklahoma State University, Stillwater, Oklahoma in December, 2010.

Name: Shoichi Ito Date of Degree: December, 2010

Institution: Oklahoma State University Location: Stillwater, Oklahoma

Title of Study: FRACTAL THZ SLOW LIGHT METAMATERIAL DEVICES

Pages in Study: 81 Candidate for the Degree of Master of Science

Major Field: Electrical Engineering

Scope and Method of Study: The goal of this study is to investigate the time delay of the fractal H metamaterials in the terahertz regime. This metamaterial contains resonators with two different sizes of H structures which mimic Electromagnetically Induced Transparency and create a transmission window and the corresponding phase dispersion, thus producing slow light. The Al structures were fabricated on silicon wafer and Mylar by using microelectronic lithography and thermal evaporation technique. By using terahertz time-domain spectroscopy, the phase change caused by the slow light system and the actual time delay were obtained. Numerical simulations were carried out to systematize the effect of permittivity and structure dimensions on the optical properties.

Findings and Conclusions: We experimentally demonstrated the numerical time delay of the fractal H metamaterial as a slow light device. When permittivity of the substrates increases, the peak position of the transmission window shifts to lower frequency and the bandwidth becomes broader. As a result, silicon performed larger time delay than that of Mylar. By changing the length of the resonator, the bandwidth and the peak position of the transmission window is controllable. At the edges of the transmission window, the negative time delays (fast light) were also observed. Mylar acts as a quaci-free standing structure and allows higher spectral measurement. Moreover, metamaterials fabricated on multiple Mylar films can potentially act as a more effective slow light device. As applications, slow light metamaterials are expected to be used for high-capacity terahertz communication networks, all-optical information processing and sensing devices.

ADVISER'S APPROVAL: Dr. Weili Zhang